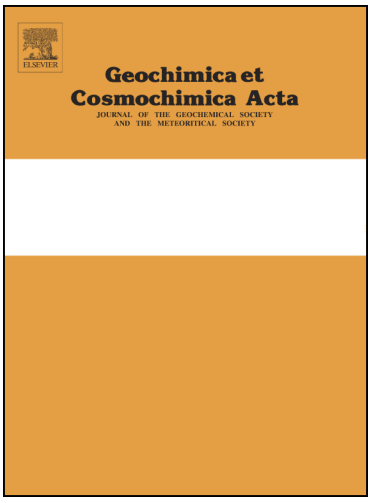

Halogens and noble gases in serpentinites and secondary peridotites: Implications for seawater subduction and the origin of mantle neon

M.A. Kendrick, M. Scambelluri, J. Hermann, J.A. Padrón-Navarta

PII: S0016-7037(18)30184-4
DOI: https://doi.org/10.1016/j.gca.2018.03.024
Reference: GCA 10718

To appear in: *Geochimica et Cosmochimica Acta*

Received Date: 3 October 2017
Accepted Date: 29 March 2018

Please cite this article as: Kendrick, M.A., Scambelluri, M., Hermann, J., Padrón-Navarta, J.A., Halogens and noble gases in serpentinites and secondary peridotites: Implications for seawater subduction and the origin of mantle neon, *Geochimica et Cosmochimica Acta* (2018), doi: https://doi.org/10.1016/j.gca.2018.03.024

Halogens and noble gases in serpentinites and secondary peridotites: Implications for seawater subduction and the origin of mantle neon

M.A. Kendrick[1,2]*, M. Scambelluri[3], J. Hermann[4] and J.A Padrón-Navarta[5]

*corresponding author; mark.kendrick@anu.edu.au

1 – Research School of Earth Sciences, Australian National University, Acton 2601, Australia.

2 – School of Earth Sciences, University of Melbourne, Victoria 3010, Australia.

3– Dipartimento di Scienze della Terra, Ambiente e Vita, Università di Genova, Italy

4 – Institute of Geological Sciences, University of Bern, Switzerland

5 – Géosciences Montpellier, Université de Montpellier, Campus Triolet cc060, Place Eugène Bataillon 34095, Montpellier cedex05, France

Words = 7660 ~~8960~~

Figures = 12 ~~14~~

Tables = 3 ~~5~~

Abstract. Ophiolitic serpentinites and secondary peridotites formed by serpentinite dehydration were investigated to improve constraints on the fates of noble gases and halogens during subduction zone metamorphism. The work extends previous studies to encompass F and four stages of serpentinization and serpentinite dehydration including: (i) oceanic serpentinites preserving the features of seafloor serpentinization; (ii) subducted high grade (olivine bearing) antigorite-serpentinites; (iii) spinifex and granofels textured chlorite harzburgites; and (iv) a garnet peridotite.

Serpentinites and secondary peridotites from different ophiolites are shown to have characteristic ranges of $^{40}Ar/^{36}Ar$: chrysotile and antigorite serpentinites from Erro Tobbio (Western Alps) have $^{40}Ar/^{36}Ar$ of ~296-390; antigorite serpentinites and chlorite harzburgites from Cerro del Almirez (Betic Cordillera) have $^{40}Ar/^{36}Ar$ of ~340-600, and chlorite harzburgites and garnet peridotites from Cima di Gagnone (Swiss Alps) have $^{40}Ar/^{36}Ar$ of ~600-1100. The variation of $^{40}Ar/^{36}Ar$ is unrelated to metamorphic grade at each locality but is broadly correlated with variation in other radiogenic isotopes ($^{206}Pb/^{204}Pb$ and $^{87}Sr/^{86}Sr$) between localities. This suggests excess ^{40}Ar was derived from terrigenous sediments with characteristic ranges of $^{40}Ar/^{36}Ar$ and $^{87}Sr/^{86}Sr$ in different subduction zones.

The secondary chlorite harzburgites have $^{20}Ne/^{36}Ar$ ratios of greater than seawater, contain parentless (or excess) ^{4}He, and have higher F concentrations than any of the serpentinites investigated. The $^{20}Ne/^{36}Ar$ is broadly correlated with $^{40}Ar/^{36}Ar$ in samples from Cerro del Almirez suggesting derivation of excess ^{40}Ar and atmospheric ^{20}Ne from a common source. The chlorite is shown to have higher concentrations of F, Ne and other noble gases than coexisting olivine and enstatite, which contain abundant desiccated fluid inclusions. The high F content and high $^{20}Ne/^{36}Ar$ ratios of the chlorite harzburgites are ascribed to fluxing of dehydrating serpentinites with F-, ^{40}Ar-, ^{4}He- and ^{20}Ne-rich fluids derived from metasediments in the subducting slab, and the inferred high compatibility of F and Ne in chlorite.

The garnet peridotite from Cima di Gagnone records the final and complete dehydration of serpentinite. Based on the analysis of mineral separates minimally affected by retrogression (marked by garnet breakdown and the appearance of Cl-rich hornblende), nominally anhydrous garnet peridotite retains Cl, Br, I and non-radiogenic noble gas concentrations up to an order of magnitude higher than average depleted mantle.

The data are consistent with serpentinised lithosphere and related secondary peridotites as major sources of deeply subducted seawater-derived volatiles in the Earth's mantle. The data also demonstrate that the relative abundances of volatiles subducted into the mantle are controlled by multiple factors including: original seafloor alteration, the relative compatibilities of different noble gases and halogens in minerals forming during different stages of subduction and chemical exchange between different lithologies during subduction. The combination of these processes has produced elevated $^{20}Ne/^{36}Ar$ in chlorite harzburgites from two unrelated localities. This suggests that subduction of atmospheric Ne could be significantly more efficient than previously realised, which has implications for interpretation of the mantles primordial $^{20}Ne/^{22}Ne$ ratio and how the Earth accreted.

1. Introduction

Halogens and noble gases are strongly concentrated in Earth's surface reservoirs of the atmosphere, seawater and sediments and therefore represent powerful elements for tracking the subduction of seawater-derived volatiles into the mantle (Holland and Ballentine, 2006; Sumino et al., 2010; Chavrit et al., 2016; Kendrick et al., 2017; Kobyashi et al., 2017; Barnes et al., 2018). Recent studies have suggested that up to ~90% of non-radiogenic Ar, Kr and Xe and most of the heavy halogens (Cl, Br, I) have subducted origins in the Earth's mantle (Holland and Ballentine, 2006; Holland et al., 2009; Mukhopadhyay, 2012; Caracausi et al., 2016; Kendrick et al., 2017). However, relatively few studies have investigated the combined behaviour of multiple halogens and/or noble gases during prograde metamorphism (John et al., 2011; Kendrick et al., 2015; 2011; Pagé et al., 2016; Pagé and Hattori, 2017), with much of what we do know about the behaviour of these elements during metamorphism based on investigations of chlorine and excess ^{40}Ar alone (e.g. Arnaud and Kelley, 1995; Scaillet, 1996; Scambelluri et al., 1997; 2004a; Philippot et al., 1998; Kelley, 2002). The current study addresses this gap in our knowledge by investigating all the noble gases (He, Ne, Ar, Kr, Xe) and halogens (F, Cl, Br, I) in a suite of high grade serpentinites and secondary peridotites formed by eclogite facies metamorphism of serpentinites (Marchesi et al., 2013; Scambelluri et al., 2014; 2015; Cannaò et al., 2015).

The investigation of noble gases and halogens in serpentinites and their metamorphosed equivalents is important because no other major subduction zone lithology is more enriched in seawater-derived Cl or H_2O (Schmidt and Poli, 1998). Furthermore, previous work has shown that serpentinites are strongly enriched in a range of fluid mobile elements including noble gases and B, which are derived mainly from seawater (e.g. Scambelluri et al., 1997; 2004b; Kendrick et al., 2013b), and in some cases a number of elements including I, As and Sb, which are usually associated with marine sediments (e.g.

Hattori and Guillot, 2007; Deschamps et al., 2012; Kendrick et al., 2013b; Cannaò et al., 2015; Scambelluri et al., 2015; Peters et al., 2017; Pagé and Hattori, 2017). The sediment-like signatures of some serpentinites can be explained by the involvement of sedimentary pore waters in serpentinisation reactions (John et al., 2011; Kendrick et al., 2011; 2013b; Pagé and Hattori, 2017), which are likely to be particularly important at the slab bend where sediments overly deep fractures into the oceanic lithosphere (Ranero et al., 2003) and in subduction channels underlying forearc environments (Bostock et al., 2002; Deschamps et al., 2013; Scambelluri et al., 2015). An implication of subduction zone serpentinites carrying 'sedimentary' signatures is that aqueous fluids produced by serpentine breakdown in subarc environments might be able to contribute toward the 'sedimentary signature' of some arc lavas (Kendrick et al., 2014; Scambelluri et al., 2015). Secondary peridotites formed by dehydration of serpentinites have also been suggested as an important component of the HIMU mantle reservoir and the principal lithology enabling subduction of noble gases and halogens into the deep mantle (Kendrick et al., 2011; 2017).

The current study extends the work of Kendrick et al. (2011, 2013b) focused on Cl, Br, I and atmospheric noble gases in serpentinites and chlorite harzburgites to include F and He and encompass four additional high grade lithologies that are key for understanding the fates of these elements in dehydrating serpentinites. The new lithologies investigated include: i) antigorite-serpentinites and ii) granofels textured chlorite harzburgites from Cerro del Almirez; and iii) a chlorite harzburgite and iv) garnet peridotite from Cima di Gagnone (Fig 1). Analysis of the new lithologies was required to better constrain the range of noble gas and halogen compositions in high grade metamorphosed serpentinites and related rocks (cf. John et al., 2011; Kendrick et al., 2011; Debret et al., 2014; Pagé and Hattori, 2017). The Cima di Gagnone garnet peridotite is of particular interest because it is the only known garnet peridotite with a demonstrable origin from dehydrated serpentinites and therefore provides

otherwise unavailable information about the nature of dehydrated lithosphere subducted into the deep mantle (Evans and Trommsdorff, 1978; Scambelluri et al., 2014; 2015).

2. Geological settings and samples

The investigated samples were selected to encompass the life cycle of serpentinites and many of the samples, as well as the sample localities, have been described in detail previously (see references below). The selected samples have been subducted to maximum depths of ~100 km (e.g. Evans and Trommsdorff, 1978; Scambelluri et al., 1997; 2004b; 2014; Trommsdorff et al., 1998; Nimis and Tromsdorff, 2001); however, the minerals investigated have wide stability fields and the rocks provide useful analogues for serpentinites subducted to much greater depths on cold geotherms (see Fig 1).

Oceanic serpentinites record initial serpentinisation at increasing distances from oceanic spreading centres and with varying involvement of sedimentary pore waters. Oceanic serpentinites include previously investigated IODP samples (Kodolányi et al., 2012; Kendrick et al., 2013b) and selected chrysotile serpentinites and serpentinised peridotites from the Monte Nero (Northern Apennines) and Erro Tobbio (Ligurian western Alps) ophiolites (Scambelluri et al., 1995; 2004b; John et al., 2011).

Antigorite serpentinites record the prograde transition of chrysotile to antigorite (Kodolányi and Pettke, 2011) and olivine-bearing antigorite serpentinites record the olivine forming dehydration reaction: antigorite + brucite => olivine + H_2O, which releases ~2 wt. % H_2O. Olivine-bearing antigorite serpentinites investigated include samples from Erro Tobbio (Scambelluri et al., 1997; 2004b; Kendrick et al., 2011) and Cerro del Almirez (Trommsdorff et al., 1998; Puga et al., 1999; Scambelluri et al., 2004a; Garrido et al., 2005; López Sanchez-Vizcaino et al., 2005; 2009; Padrón-Navarta et al., 2011).

Chlorite harzburgites record the final breakdown of antigorite by the reaction: antigorite => olivine + enstatite + chlorite + H_2O, which releases ~5-10 wt. % H_2O. Chlorite harzburgites include samples from both Cerro del Almirez and Cima di Gagnone (Evans and Trommsdorff, 1978; Padrón-Navarta et al., 2011; 2013; Scambelluri et al., 2001; 2014; Trommsdorff et al., 1998). The chlorite harzburgites from Cerro del Almirez are divided into two textural types that reflect different rates of reaction progress and fluid escape, one has brown skeletal olivine defining a 'spinifex-like texture' and the second type has a granofels texture (Figs 2a and b; Padrón-Navarta et al., 2011; 2015). Chlorite-rich veins from this locality are related to the escape of antigorite breakdown fluids.

Garnet peridotite records the final dehydration of chlorite harzburgites by the reaction: chlorite + enstatite ± diopside => garnet + olivine + H_2O, which releases ~1-5 wt. % H_2O. The garnet peridotite investigated came from outcrop Mg160 at Cima di Gagnone (Evans and Trommsdorff, 1978; Scambelluri et al., 2014; 2015). The garnet peridotite probably records the same metamorphic conditions as the chlorite harzburgite from Cima di Gagnone but occurs in a different lens within the gneiss that had different protolith composition (Fig 1; Nimis and Tromsdorff, 2001; Scambelluri et al., 2014).

Desiccated fluid inclusions associated with the escape of fluids from the dehydrating serpentinites are preserved in the nominally anhydrous secondary olivine, enstatite and garnet in samples from both Cerro del Almirez and Cima di Gagnone (Scambelluri et al., 1997; 2004b; 2015; Kendrick et al., 2011). The inclusions have been desiccated by the escape of H^+ ions and/or reaction with the host mineral, but they retain solutes including heavy noble gases representative of the originally trapped fluids (Scambelluri et al., 2004b; 2015; Kendrick et al., 2011). Some photomicrographs of representative textures and fluid related inclusions are shown in Fig 2.

3. Methods

Halogens and noble gases were measured by a variety of techniques. Chlorine was measured in a thin section of Mg160 by electron microprobe. Halogens (Cl, Br and I) and noble gases (Ar, Kr, Xe) were analysed in irradiated samples using extended ^{40}Ar-^{39}Ar methodology and He and Ne were analysed separately in non-irradiated sample aliquots (whole rocks and mineral separates). Fluorine was measured by SHRIMP in mineral separates and whole rocks prepared as flux glasses.

3.1 Halogens by electron microprobe and the noble gas method

The JEOL 8530 plus electron microprobe in the Centre of Advanced Microscopy at the Australian National University (ANU) was used to investigate the distribution of Cl in sample Mg160, which is a unique garnet peridotite of critical importance to this study. The analytical conditions for EPMA included an accelerating potential of 15 keV, beam current of 20 nA and a 8 μm spot size. Counting times during the main analytical session were 10 seconds for the majority of elements and 30 seconds for Cl, which gave a calculated Cl detection limit of ~30 ppm. Scapolite BB1 with 3.1 wt. % Cl was used as the Cl calibration standard (Kendrick, 2012) and Durango apatite analysed as an unknown gave a Cl concentrations within the previously reported range (Marks et al., 2012; Nadzri et al., 2017).

The concentrations of Cl, Br and I were measured in high purity mineral separates and crushed samples (0.2-1 mm size, not powders) intended to approximate whole rocks. These measurements were made using the noble gas method, which is an extension of the ^{40}Ar-^{39}Ar methodology and has sub-ppm detection limits for Cl and sub-ppb detection limits for Br and I (Kendrick, 2012; Kendrick et al., 2013a). Sample chips (0.2-1 mm size) were ultrasonically washed in distilled water and acetone and 23-56 mg sized portions were packed in Al-foil and

placed in silica glass irradiation canisters along with the ^{40}Ar-^{39}Ar flux monitor Hb3gr (Roddick, 1983) and aliquots of 3 scapolite gems (Kendrick, 2012; Kendrick et al., 2013a). The samples were irradiated in two batches: UM#44 (42 hours in position 5c of the McMaster reactor on the 27th February 2011) and UM#53 (80 hours in a central position of the USGS Triga reactor on the 28th November 2012). The samples received total neutron fluences of 1.2×10^{19} neutrons cm^{-2} in irradiation UM#44 and 7×10^{18} neutrons cm^{-2} in irradiation UM#53.

The irradiated samples were returned to the noble gas laboratory and analysed within 1 year of irradiation. The samples were placed in Sn-foil packets in an ultra-high vacuum sample holder and baked at ~120 °C for 24 hours to achieve ultra-high vacuum. Each sample was successively dropped into the tantalum resistance furnace and noble gases were extracted in 20 minute heating steps, encompassing a low temperature step (300 or 400 °C) and a high temperature step (1500 or 1600 °C). The extracted gases were purified using a Ti-foil bulk getter at 700 °C and a series of three SAES getters over a period of 1 hour. The purified noble gases were then expanded into the MAP 215-50 noble gas mass spectrometer, and analysed for irradiation-produced and naturally occurring isotopes of Ar, Kr and Xe. The measurements were made in static vacuum in 9 cycles of peak jumping over a period of ~50 minutes.

The abundances of Cl, Br, I, K and Ca were calculated from signals of irradiation-produced $^{38}Ar_{Cl}$, $^{80}Kr_{Br,}$ $^{128}Xe_{I,}$ $^{39}Ar_{K}$ and $^{37}Ar_{Ca}$ based on mass spectrometer sensitivity determined via daily air calibrations and noble gas production ratios ($^{38}Ar_{Cl}$/Cl, $^{80}Kr_{Br}$/Br, $^{128}Xe_{I}$/I, $^{39}Ar_{K}$/K, $^{37}Ar_{Ca}$/Ca) determined from the irradiation monitors (Kendrick, 2012; Kendrick et al., 2013a). Standard corrections were made for instrument blanks, ^{37}Ar decay and Ar interference reactions (see Kendrick, 2012). Elemental ratios have typical analytical precision of 1-2%, but the long term reproducibility of elemental abundances, relevant for

comparing data between different irradiations and different techniques is estimated as 10% (2σ) (see Kendrick et al., 2013a).

3.2 Fluorine by SHRIMP-II

The SHRIMP-II housed at the ANU was used to measure F signals in individual grains of chlorite, garnet, olivine and pyroxene separated from the chlorite harzburgites and garnet peridotite. In addition, SHRIMP-II was used to measure F in Li-metaborate glasses produced by flux melting various whole rock sample powders following standard XRF protocols (see Kendrick et al., 2018). The analysis of flux glasses was undertaken to test if SHRIMP could be used to measure F in whole rocks as well as mineral separates in a single analytical session. Possible matrix affects and F-loss from Li-metaborate glasses was evaluated by preparing Li-metaborate glasses of F-doped MORB and producing a F-doped MORB glass in a piston cyclinder at 1250 °C and 6 kbar.

Chips of flux glasses, standards and mineral separates were mounted in epoxy and polished to a 1 µm finish. The polished mount was cleaned with acetone, dried overnight in a vacuum furnace at 100 °C and given a 10 nm thick gold coat before loading into the SHRIMP II for analysis. The sample mount was held in the SHRIMP-II ultrahigh-vacuum chamber at a potential of 10 kV and targeted with a primary Cs^+ ion beam focused to a ~30 µm spot on the sample. The ion beam generated with a Kimball Physics Cs gun (IGS-4) was 2 nA and had an energy of 5 kV, giving a total impact energy of 15 keV. Charge compensation was achieved by focusing a 2 kV electron beam generated with a Kimball Physics electron gun onto the sample mount. Secondary ^{19}F and ^{18}O released from the sample were measured by Faraday multi-collection (10^{11} and 10^{12} resistors). The instrument was configured to give resolution of 5,000 (1% valley definition). Data was collected over four 20 s integration periods in static mode (total measurement time 80 s).

The measured ^{19}F signal was calibrated using ^{18}O as an internal standard and a calibration curve constructed with F-doped Li-metaborate flux glasses (Fig S1). This calibration gave F concentrations of 279 ± 1 ppm in NIST SRM 610 (n = 2), 330 ± 40 ppm in RGM-2 (n = 3, flux glass) and 1150 ppm in JR-1 (flux glass) that are all within uncertainty of previous analyses (Hoskin, 1999; Michel and Villemant, 2003; Balcone-Boissard et al., 2009; Kendrick et al., 2017; see Kendrick et al. (2018) for details). The SHRIMP analyses have a ppm-level detection limit in mineral grains and glasses and are repeatable at the 1-2% level. However, the presence of minor F in the Li-metaborate flux (e.g. a blank) means that the effective detection limit of F in whole rocks analysed as flux glasses is 20 ppm. Matrix affects between minerals and the calibration standards are estimated as <10% (below).

3.3 Noble gas analysis in non-irradiated samples

Portions of non-irradiated mineral separates (~100-500 mg), and unsorted mineral grains approximating whole rocks, were ultrasonically washed in acetone and distilled water. After drying they were then wrapped in Sn-foil sample packets and loaded into an ultra-high vacuum sample carasol attached to a resistance furnace on the VG5400 noble gas mass spectrometer at the ANU. The non-irradiated samples were baked overnight at ~200-220 °C to achieve ultra-high vacuum and outgassed in a single 30 minute heating step at 1800 °C. The extracted gases were purified using two Ti-foil bulk getters and a SAES getter over a period of at least 2.5 hours. The purified gas was condensed onto a cryogenic head at 33 K and each noble gas was sequentially released and isotopically analysed in the VG 5400 noble gas mass spectrometer. Small corrections were made for instrumental blank and interference of $^{40}Ar^{++}$ on ^{20}Ne and CO_2^{++} on ^{22}Ne. The methods have been described previously by Honda et al. (2004).

4. Results

The halogen data obtained by the electron microprobe, SHRIMP and noble gas method are summarised in section 4.1 and Table 1, where the whole rock Cl, Br, I and K concentrations determined by the noble gas method are based on total fusion. In contrast, in order to minimises the influence of atmospheric contamination, the whole rock noble gas abundance data summarised in section 4.2 and Table 2 are based on high temperature heating steps (below). An identical approach has been applied to the new data reported here for the first time and data from previous studies (Kendrick et al., 2011; 2013b); and all the Br and I data are normalised to the revised scapolite standard values of Kendrick et al. (2013ab). The dataset is tabulated fully in the electronic supplement.

4.1 Halogens

The majority of chrysotile- and antigorite-serpentinites from ophiolites have F concentrations of less than the 20 ppm limit of reliable measurement in whole rock flux glasses. Fluorine was just detectable in samples MN5 from Monte Nero and Alm-94 from Cerro del Almirez, which each contain ~20 ppm F (Table 1). These results are consistent with previous work, which indicated 1-18 ppm F in serpentinites from Erro Tobbio and 14-30 ppm F in serpentinites from Monte Nero (John et al., 2011). The oceanic serpentinites contain 330-2300 ppm Cl (Table 1; Kendrick et al., 2013b) that are typical of seafloor serpentinites (Kendrick, 2018). The concentrations of Br and I increase from minima of 17 ppb I and 1.3 ppm Br to maxima of 24 ppm Br and 45 ppm I in serpentinites formed proximally to sediments, including those formed in forearc environments (Table 1; Kendrick et al., 2013b). The antigorite-serpentinites from Cerro del Almirez have 160-250 ppm Cl, 170-300 ppb Br and 13-24 ppb I, which overlap the ranges reported for antigorite-serpentinites from Erro Tobbio (Kendrick et al., 2011) and are lower than is typical of oceanic serpentinites (Fig 3; Table 1).

The granofels and spinifex textured chlorite harzburgites from Cerro del Almirez and Cima di Gagnone have similar ranges of 38-170 ppm F, 36-380 ppm Cl, 110-810 ppb Br and 4-72 ppb I (Table 1; electronic supplement). Most of the chlorite harzburgites are depleted in Cl, Br and I, but enriched in F relative to the serpentinites investigated (Fig 3; Table 1). SHRIMP analysis indicates that within sample Al08-16, chlorite contains 220-280 ppm F, olivine 9-28 ppm F and enstatite ~5 ppm F (Table 1; electronic supplement). Furthermore, the whole rock F estimated on the basis of these concentrations and modal mineralogy is similar to that measured in a flux glass prepared from this sample (Table 1; electronic supplement). This suggests that matrix affects associated with F measurement are negligible and that chlorite is the dominant host of F in this sample, with negligible F in either fluid inclusions or Ti-clinohumite, which locally contains up to 2 wt.% F in some chlorite harzburgites (Puga et al., 1999; Garrido et al., 2005; López Sanchez-Vizcaíno et al., 2005; Scambelluri et al., 2014). In contrast, the heavy halogens (Cl, Br and I) have similar concentrations in chlorite (140-150 ppm Cl, 130-200 ppb Br and 42-47 ppb I) and olivine and enstatite (170-240 ppm Cl, 220-340 ppb Br and 22-29 ppb I), which are likely to contain Cl, Br and I in desiccated fluid inclusions (Fig 3; Table 1).

The garnet peridotite (Mg160) has a calculated F concentration of ~11 ppm that is based on measured concentrations of 5±1 ppm F in garnet, 10±5 ppm in clinopyroxene, ~13±2 ppm F in olivine and a modal mineralogy of 50 ol: 15 en; 25 grt: 10 cpx(+ hbl). As a result, F was too low to measure in a flux glass of this sample (Table S4 electronic supplement). The garnet peridotite contains 20 ppm Cl in a combined olivine-enstatite mineral separate, 78 ppm Cl in a garnet separate and 290 ppm Cl in a clinopyroxene separate that contains up to ~10% retrograde hornblende. The retrograde hornblendes have variable compositions with ~0.1-0.5 wt. % Cl (Table S5 electronic supplement), and the hornblende is found replacing both garnet and clinopyroxene (Fig 6). However, its green colouration meant

that it was concentrated in the clinopyroxene mineral separate. It was easily separated from the pink garnet during hand picking and the concentration of 78 ppm Cl in the garnet separate is attributed to the presence of Cl-rich desiccated fluid inclusions in this mineral that are related to peak metamorphism and have been documented previously (Scambelluri et al., 2015).

The original Cl, Br and I contents of the peak metamorphic garnet peridotite are estimated as ~40 ppm Cl, ~180 ppb Br and ~9 ppb I based on the model mineralogy (50 ol: 15 en; 25 grt: 10 cpx(+ hbl)), but excluding the contaminated clinopyroxene mineral separate (Table 1). The estimated peak metamorphic concentrations of Cl, Br and I are 20-30% lower than in the retrograded sample, and similar to the values measured in the chlorite harzburgite from Cima di Gagnone (Table 1).

4.2 Noble gases

The noble gas concentrations reported for irradiated samples are based on high temperature heating steps and do not include gases released in the 300 or 400 °C step (Table 2; electronic supplement). This approach was adopted to minimise the effects of atmospheric contamination, which is incompletely removed from sample surfaces during baking at 120 °C in vacuum prior to analysis. In contrast, non-irradiated samples were baked at ~200-220 °C in vacuum prior to analysis and analysed in a single heating step. Atmospheric contamination is a perennial problem in noble gas studies and it is impossible to eliminate entirely. Differences between duplicate sample aliquots, including the low $^{40}Ar/^{36}Ar$ and high ^{36}Ar concentration of the irradiated Mg31 09-03 aliquot (Table 2) relative to the unirradiated aliquot of this sample (Table 3) could be attributed to either sample heterogeneity or persistent air contamination. However, several observations suggest that the approaches

adopted here have minimised the influence of atmospheric contamination and the tabulated results can be considered fairly representative of the samples uncontaminated composition.

Firstly, while gases released at 300-400 °C typically have an atmospheric $^{40}Ar/^{36}Ar$ ratio (Table S1 electronic supplement), the gases released at 1500-1800 °C from many of the irradiated and non-irradiated samples have non-atmospheric $^{40}Ar/^{36}Ar$ ratios that cannot be ascribed to atmospheric contamination (Table 2 and 3). Furthermore, the lowest measured $^{40}Ar/^{36}Ar$ ratios are obtained for seafloor serpentinites and $^{40}Ar/^{36}Ar$ varies systematically between the ophiolite localities encompassing ranges of ~296-390 in samples from Erro Tobbio, ~320-650 in samples from Cerro del Almirez and a representative range of ~600-1100 in samples from Cima di Gagnone (Fig 5). Note that the lower limit of $^{40}Ar/^{36}Ar$ in Cima di Gagnone samples is based on the non-irradiated aliquot of Mg31 09-03 with a $^{40}Ar/^{36}Ar$ of 646 ± 2 and that the lower value in the irradiated aliquot is attributed to atmospheric contamination (cf. Tables 2 and 3). The representative ranges are broadly related to other radiogenic isotopes at each locality (Fig 5; Cannaò et al., 2015; Harvey et al., 2014), consistent with the measured $^{40}Ar/^{36}Ar$ ratios being representative of sediment-influenced fluids responsible for original serpentinisation on either the seafloor or in former subduction zones at each locality (Table 2; Kendrick et al., 2013b; 2011). The preservation of initial $^{40}Ar/^{36}Ar$ ratios occurs because the samples contain very little K (e.g. ppm-levels or less; Table 1). Furthermore, retrograde hornblende in sample Mg160 does not influence the whole rock ^{40}Ar-^{39}Ar systematics of this sample (Fig 6).

A second line of reasoning that supports the measured noble gas concentrations as being fairly representative of the samples is that the concentrations of ^{36}Ar and other noble gases decrease systematically from maximums of 80-5,400×10^{-15} mol/g ^{36}Ar in oceanic serpentinites, to concentrations of 65-750×10^{-15} mol/g ^{36}Ar in antigorite-serpentinites, to concentrations of 9-640×10^{-15} mol/g ^{36}Ar in granofels and spinifex textured chlorite

harzburgites, to low concentrations of 25-46×10^{-15} mol/g ^{36}Ar in olivine and garnet separated from the garnet peridotite (which were not affected by retrograde alteration; Fig 7; Table 2 and 3). In addition, the broad correlation between ^{36}Ar and Cl concentration is in line with expected volatile loss during metamorphism (Fig 8). Finally, we show below that relationships between ^{40}Ar/^{36}Ar and the relative abundances of different atmospheric noble gases (^{20}Ne, ^{36}Ar, ^{84}Kr and ^{130}Xe; Fig 7) cannot be explained by atmospheric contamination.

Interestingly, chlorite mineral separates have much higher concentrations of ^{36}Ar (210-640×10^{-15} mol/g ^{36}Ar) and ^{20}Ne than the olivine-enstatite separates (9.4-70×10^{-15} mol/g ^{36}Ar) (Table 3; electronic supplement). This is despite the olivine-enstatite separates, which contain desiccated fluid inclusions, having the higher Cl concentrations (170-240 ppm; section 4.1). These data suggest that while fluid inclusions are a dominant reservoir for heavy halogens in chlorite harzburgites, the mineral structure including inter-layer sites in chlorite are of equal or slightly greater importance for hosting noble gases (Fig 9).

All the samples have Ne, Kr and Xe isotope signatures within uncertainty of air. All the samples investigated for helium isotopes have ^{3}He below the detection limit but are enriched in ^{4}He relative to air (Table 3). A detailed consideration of the ^{4}He budget is beyond the scope of the current contribution. However, based on Alpine ages for peak metamorphism (15-45 Ma) and likely upper limits for U and Th (Table S3; electronic supplement), it appears that while most of the serpentinites have lost ^{4}He and are dominated by in situ ^{4}He produced by U and Th decay, the antigorite-serpentinites from Cerro del Almirez and the secondary peridotites from both Cerro del Almirez and Cima di Gagnone contain substantial amounts of trapped excess ^{4}He that is unlikely to have been produced in situ. The estimated ratio of excess ^{4}He to excess ^{40}Ar in these samples (^{4}He/^{40}Ar*) varies from 2 to 45 that is within the range of crustal fluids (Table S3; electronic supplement).

5. Discussion

The new data provide some important insights on the life cycle of serpentinites including the types of fluid responsible for initial serpentinisation and evidence for chemical exchange with metasediments in subduction zones. The new data are also of particular importance for constraining what might be returned into the deep mantle in dehydrated serpentinites. These issues and the implications of subducting atmospheric Ne for models of planetary accretion are addressed below.

5.1 The origin of serpentinising fluids

The fluids responsible for serpentinisation reactions are commonly derived from seawater but have evolved by interaction with sediments and/or crustal lithologies to different degrees. The involvement of sediments increases away from oceanic spreading centres. In addition, the nature of the sediments differs from largely marine in oceanic settings, with abundant I-rich organic matter, to terrigenous sediments with elevated concentrations of incompatible and radioactive elements closer to continental margins (Plank and Langmuir, 1998).

Serpentinites formed close to spreading centres have I/Cl similar to average crust and $^{40}Ar/^{36}Ar$ of close to the atmospheric/seawater value of 296 (Table 2 and 3; Kendrick et al., 2013b). In contrast, the increasing influence of organic-rich sediments is reflected by the very high I/Cl ratios of serpentinites from some forearc settings, the Monte Nero ophiolite (Fig 10; John et al., 2011; Kendrick et al., 2013b) and serpentinies from the Dominican Republic (see Pagé and Hattori, 2017). The increasing influence of continentally-derived sediments enriched in incompatible and radioactive elements like K (and Rb) is seen in the higher $^{40}Ar/^{36}Ar$ ratios of serpentinites and secondary peridotites from ophiolites (Fig 5; Table 2 and 3).

In contrast with Cl, Br and I, which have high solubilities in seawater and sedimentary pore waters, the majority of serpentinites investigated have low concentrations of <20 ppm F (Fig 3; Table 1) and similarly low F concentrations have been reported for oceanic serpentinites preserved in the Dominican Republic ophiolite (Pagé and Hattori, 2017). The low F content of many oceanic serpentinites is explained because seawater contains only 1.3 ppm F (Drever, 1997), and even though carbonate rich sediments can contain 1000-1500 ppm F (Rude and Aller, 1991), the low solubility of F under diagenetic conditions (Seyfried and Ding, 1995) means it retains a low seawater-like concentration in most sedimentary pore waters (Gieskes et al., 2002). Higher concentrations of >100 ppm F reported in some previous studies of serpentine minerals can therefore only be generated at very high water/rock ratios (Debret et al., 2014) and are not necessarily representative of bulk serpentinites.

The serpentinites have $^{20}Ne/^{36}Ar$, $^{84}Kr/^{36}Ar$ and $^{130}Xe/^{36}Ar$ ratios that are fractionated around the seawater values and encompass similar ranges as sediments and sedimentary pore waters (Fig 11; Podosek et al., 1980; Matsuda and Nagoa, 1986; Pitre and Pinti, 2010). Fractionated noble gas abundance ratios are probably generated from seawater during trapping in some oceanic serpentinites. However, the involvement of sediment pore waters with variable $^{20}Ne/^{36}Ar$, $^{84}Kr/^{36}Ar$ and $^{130}Xe/^{36}Ar$ ratios is supported by the elevated I/Cl and $^{40}Ar/^{36}Ar$ ratios of many serpentinites (Figs 5 and 10). In addition, the broad correlation between $^{20}Ne/^{36}Ar$ and $^{40}Ar/^{36}Ar$ in samples from Cerro del Almirez suggests excess ^{40}Ar (and ^{4}He) and atmospheric ^{20}Ne were introduced into chlorite harzburgites together in sediment- or meta-sediment derived fluids in this location (Fig 11c).

In addition to the elevated $^{20}Ne/^{36}Ar$ ratio (Fig 11c), chlorite harzburgites from Cerro del Almirez and Cima di Gagnone have elevated concentrations of 36-170 ppm F (Fig 3) and excesses of ^{4}He (Table S3; electronic supplement). We note that high F concentrations can

be generated in serpentinites at a sufficiently high water/rock ratios (Debret et al., 2014), but the antigorite serpentinites from Cerro del Almirez contain <20 ppm F (Fig 3; Table 1). Based on our data we suggest that high F concentrations (e.g. more than ~ 40 ppm F) and high $^{20}Ne/^{36}Ar$ ratios are not typical characteristics of bulk serpentinites formed on the seafloor. Rather it seems these characteristics are more likely to be acquired in antigorite-serpentinites and chlorite-harzburgites during subduction zone metamorphism where F has a much higher mobility than on the seafloor (see also Pagé and Hattori, 2017). As already noted, the localised presence of F-rich Ti-clinohumite provides evidence that F was mobilised during eclogite facies metamorphism at Cerro del Almirez (e.g. Puga et al., 1999; López Sanchez-Vizcaino et al., 2005) and introduction of F from an external source is arguably favoured by the especially high F content of Ti-clinohumite adjacent to ophicarbonates on the edges of the chlorite harzburgite (Puga et al., 1999; López Sanchez-Vizcaíno et al., 2005). The abundances of other fluid mobile trace elements and the $\delta^{11}B$ and $^{87}Sr/^{86}Sr$ isotope signatures of the chlorite harzburgites at Cerro del Almirez and Cima di Gagnone also suggest influx of sediment-derived fluids during antigorite breakdown and progressive subduction (Fig 5; Marchesi et al., 2013; Harvey et al., 2014; Cannaò et al., 2015).

The high diffusivity of light noble gases relative to heavy noble gases means that on average metamorphic fluids should be characterised by high $^{20}Ne/^{36}Ar$ ratios (Kendrick and Burnard, 2013). Therefore, the F enrichment and the coupled $^{20}Ne/^{36}Ar$ and $^{40}Ar/^{36}Ar$ ratios of the chlorite harzburgites investigated (Fig 11c) are interpreted to provide evidence for metasediment-derived fluids fluxing the dehydrating serpentinites. The signatures are preserved in the chlorite harzburgite because as inferred from the mineral concentration data (Fig 9), F and noble gases have relatively high compatibilities in chlorite (below). The proposed chemical exchange between dehydrating serpentinites and metasediments during subduction is facilitated because the lithologies investigated were exhumed from subduction

channels, where fluids flux up the interface of the downgoing slab and mantle, and where rock types with contrasting compositions are juxtaposed in close proximity (e.g. Deschamps et al., 2013; Scambelluri et al., 2014).

5.2 Siting of noble gases and halogens in serpentinites and related rocks

Serpentinites are typically very fine grained and do not contain microscopically visible fluid inclusions. The high concentrations of Cl, Br and I in seafloor serpentinites therefore suggests that all the halogens can either substitute for the OH-group in chrysotile/lizardite or that they are efficiently trapped in nano-porosity between serpentine minerals (Anselmi et al., 2000; Plumper et al., 2012; Lafay et al., 2016). Vacant ring sites in the serpentine lattice (and other hydrous minerals) have been experimentally demonstrated as important hosts for noble gases (Jackson et al., 2013; 2015) and noble gases could also be stored along grain boundaries and in nano-porosity between serpentine minerals. In contrast, desiccated fluid inclusions have been observed in many of the nominally anhydrous minerals formed by antigorite breakdown (e.g. Fig 2f; Scambelluri et al., 1997; 2004b; 2015) and have been suggested as important reservoirs for noble gases and halogens in secondary peridotites (Kendrick et al., 2011).

Our new data suggest the relative importance of desiccated fluid inclusions is different for noble gases, F and heavy halogens: chlorite in samples Al08-16 and Al10-06 contains very few visible fluid inclusions but it has concentrations of noble gases that are 5-10 times higher, F concentrations that are 10-20 times higher and Cl, Br and I concentrations that are similar to the more abundant olivine and enstatite minerals (Tables 1, 3 and 4). As a result, on a whole rock basis, chlorite with an estimated modal abundance of ~15% is the

dominant host of F and Ne, and of approximately equal importance as fluid inclusions in olivine and enstatite for hosting heavy noble gases (Fig 11).

The high concentration of noble gases in chlorite is consistent with the high compatibility of Ar in other sheet silicates under high pressure metamorphic conditions (Kelley, 2002). Furthermore, the chlorite has slightly higher $^{20}Ne/^{36}Ar$ than the olivine-enstatite (Tables 4; Fig 13), which is consistent with preferential storage of light noble gases in ring sites (Jackson et al., 2013), although interlayer sites are probably of additional importance in sheet silicates. The relatively high concentrations of Cl, Br and I in chlorite suggest that these large halide ions are able to substitute for the OH-group in chlorite formed under eclogite facies conditions (Table 1). However, desiccated fluid inclusions in olivine and enstatite are the dominant host of heavy halogens (Cl, Br and I) on a whole rock basis (Fig 11).

5.3 The evolving composition of the subducting slab

The general progression toward lower concentrations of noble gases, Cl, Br and I from oceanic serpentinites to antigorite serpentinites, chlorite harzburgites and garnet peridotite (Figs 3, 7 and 8) is in line with the expected loss of volatiles during metamorphic dehydration. However, there are additional subtle changes in the relative abundance ratios of the different volatiles, which may be significant but are difficult to assess because of the small number of high grade samples available for investigation and the impossibility of establishing exact equivalence between rocks of different grade (even when they occur at the same locality).

Firstly, oceanic serpentinites from forearc and ophiolite settings including Monte Nero and Erro Tobbio have much higher I/Cl and Br/Cl ratios than any of the high grade

antigorite serpentinites or secondary peridotites investigated, including antigorite serpentinites from Erro Tobbio (Fig 10; Kendrick et al., 2013b). This is consistent with preferential loss of Br and I relative to Cl during antigoritisation of chrysotile and/or the reaction, antigorite + brucite => olivine + H_2O (Fig 1; Kendrick et al., 2011). Preferential loss of I relative to Cl during antigoritisation might also be able to generate fluids with very high I/Cl ratios, that could help account for the highest measured I/Cl ratios in forearc serpentinites that are higher than typical sedimentary pore waters (Fig 10a) and are related to slab fluids, which can have very variable composition (cf. Pagé and Hattori, 2017). In contrast, the new data show that antigorites and chlorite harzburgites from Cerro del Almirez have similar ranges of Br/Cl and I/Cl (Fig 10), demonstrating that Br/Cl and I/Cl were not significantly fractionated during the final breakdown of antigorite at this locality (cf. Kendrick et al., 2011). The lack of fractionation during the final breakdown of antigorite is probably explained because heavy halogens are not fractionated by trapping in fluid inclusions and desiccated fluid inclusions are the dominant reservoir of Cl, Br and I in secondary peridotites (Fig 9). In contrast with the heavy halogens, the chlorite harzburgites have higher F concentrations and F/Cl ratios than lower grade serpentinites (John et al., 2011), including the antigorite serpentinites from Cerro del Almirez (Table 1). Our preferred explanation for this is that F was introduced into the chlorite harzburgites from metasedimentary lithologies (along with excess ^{40}Ar, excess ^{4}He and atmospheric ^{20}Ne) during subduction (section 5.1).

The average $^{84}Kr/^{36}Ar$ and $^{130}Xe/^{36}Ar$ ratios of the serpentinites and related rocks are scattered around the values of seawater and sedimentary pore waters providing little evidence for fractionation during subduction (Fig 11a). However, secondary peridotites have unexpectedly high average $^{20}Ne/^{36}Ar$ ratios of 0.21-0.25 that are significantly higher than the average serpentinite values of 0.1-0.11 (Fig 11a; Table 3). This difference cannot be

explained by diffusion related gas loss because diffusion would produce fluids with high $^{20}Ne/^{36}Ar$ ratios and residual rocks with low $^{20}Ne/^{36}Ar$ ratios. The range of $^{20}Ne/^{36}Ar$ in secondary peridotites overlaps sedimentary pore waters (Fig 11b) and the broad trend between $^{20}Ne/^{36}Ar$ and $^{40}Ar/^{36}Ar$ (Fig 11c) implies that high $^{20}Ne/^{36}Ar$ ratios are explained by fluid interaction and chemical exchange with ^{40}Ar- (and ^{4}He-) bearing (meta)sediments. The data in Fig 11c clearly show that the high $^{20}Ne/^{36}Ar$ ratios cannot be ascribed to atmospheric contamination, because they are associated with some of the highest measured $^{40}Ar/^{36}Ar$ ratios that are distinct from air.

5.4 Volatiles returned to the mantle

The investigated sample of garnet peridotite from outcrop Mg160 does not contain primary amphibole, which has been previously identified in samples from this outcrop on the basis of textural relationships and REE abundance patterns (Pfiffner and Trommsdorff, 1998; Scambelluri et al., 2014). Textural relationships show that hornblende in the sample investigated has a secondary origin (Fig 4). The documentation of only retrograde secondary hornblende is consistent with the original proposition of Evans and Tromsdorff (1978) that an assemblage of grt + en + cpx + olv (assemblage I) was overprinted by a later assemblage of grt + en + cpx + olv + hbl (assemblage II) at this locality. It is also consistent with geobarometric constraints that indicate the outcrop reached a metamorphic peak straddling the ~3 GPa phase transition between amphibole-free and amphibole-bearing garnet peridotite (Fig 1; Nimis and Trommsdorff, 2001). Given the absence of peak metamorphic amphibole in the sample investigated (Fig 4), it is reasonable to estimate the peak metamorphic concentrations of halogens and noble gases in this sample based on the olivine and garnet mineral separates alone, which are free of retrograde alteration (Tables 1 and 3).

The concentrations of halogens and noble gases in the peak metamorphic garnet peridotite are estimated as about ten times greater than the concentrations of these elements in average depleted mantle (Figs 3 and 7; Tables 1 and 3). However, it should be noted that these figures represent absolute minimums for the return flux of volatiles into the deep mantle in altered slab lithosphere. The actual flux, and the relative abundances of the different volatiles in the slab lithosphere, will depend on the hydration state of the slab as it passes beneath the magmatic arc and volatiles become isolated in the down going slab. Seismic evidence suggests that in cold slab geotherms antigorite can be subducted to depths as great as 250 km (Green II et al., 2010). In such cases it is likely that when the antigorite breaks down halogens and noble gases will be partially retained in fluid inclusions trapped in nominally anhydrous minerals (Fig 2f) and in the crystal structures of hydrous minerals like chlorite or phase A (Fig 1), and that these volatiles could then be subducted very deeply into the mantle (Kendrick et al., 2011). The long-term retention of noble gases and halogens in subducting slabs is also made more likely by the increasing solubility of H_2O in nominally anhydrous minerals, including olivine polymorphs, with depth (Kohlstedt et al., 1996). A recent experimental study has shown that in addition to fluid inclusions (Fig 2f; Scambelluri et al., 2015), about 50 ppm H_2O is incorporated into the lattice of olivine after the breakdown of chlorite (Padrón-Navarta and Hermann, 2017). An even greater amount of H_2O would be expected in the lattice of olivine formed at greater depths by the eventual breakdown of Phase A on cold slab geotherms (cf. Fig 1). The dissolution of water in nominally anhydrous minerals and the lack of further dehydration reactions prevent the formation of free fluids meaning that noble gases and halogens cannot be easily advected away from deeply subducted slabs. Similarly, noble gases (and halogens) are retained in eclogite facies lithologies during exhumation because exhumation occurs rapidly and in the absence of free fluids (e.g. Kelley, 2002).

If Cl, Br and I have a dominantly subducted origin in the mantle (e.g. Kendrick et al., 2017), then on average, the slab residue subducted beyond the arc must have Br/Cl and I/Cl ratios similar to the mantle (cf. Fig 10). In contrast, the secondary peridotites investigated here have Br/Cl of both higher and lower than the mantle range, and I/Cl that extends from mantle to higher values (Fig 10; Table 1). There are too few secondary peridotites available for analysis to determine the average Br/Cl and I/Cl of subducted slab lithosphere. However, we propose that a major role for serpentinites and secondary peridotites in facilitating halogen subduction into the deep mantle is consistent with: i) the scattered Br/Cl and I/Cl data of the available secondary peridotites overlapping the compositional range of the mantle, and ii) the general trend of secondary peridotites to have lower Br/Cl and I/Cl than serpentinites, which favours preferential subduction of Cl relative to Br and I (Kendrick et al., 2011). In addition, when halogens in other slab lithologies including altered gabbros and basalts are included, it seems feasible that the average Br/Cl and I/Cl of subducting slabs could be close to that of the mantle (Fig 10). However, further work is required to understand how these signatures are blended together to produce a relatively limited range of Br/Cl and I/Cl in the mantle (Kendrick et al., 2017).

The average noble gas composition of the subducting slab has previously been suggested to contain negligible ^{20}Ne and have $^{84}Kr/^{36}Ar$ and $^{130}Xe/^{36}Ar$ ratios of similar to, but slightly higher than, seawater (Holland and Ballentine, 2006; Smye et al., 2017). In contrast, the current study shows that despite the low solubility of He and Ne in seawater, secondary peridotites formed by serpentine breakdown at two unrelated localities are both characterised by small excesses of ^{4}He and high $^{20}Ne/^{36}Ar$ ratios of much greater than seawater (Fig 11; Table S3 electronic supplement). Therefore the relative solubilities of different noble gases in seawater are only one of many controls on the subduction potential of different noble gases. The current data suggest that subduction of atmospheric Ne might be

significant, but because of the mantles high $^{4}He/^{20}Ne$ ratio, subduction of radiogenic ^{4}He is not important.

5.5 *Implications for Earth's accretion*

Non-radiogenic isotopes of Ar, Kr and Xe are believed to have a dominantly subducted origin in the Earth's mantle (Trieloff et al., 2000; Holland and Ballentine, 2006; Holland et al., 2009; Mukhopadhyay, 2012; Caracausi et al., 2016). However, the low solubility of Ne in seawater coupled with the similarity of the maximum measured $^{20}Ne/^{22}Ne$ ratio in mantle materials (~12.5-12.9; Yokochi and Marty, 2004; Mukhopadhyay, 2012; Péron et al., 2016; 2017) and Ne implanted in meteorites (Ne-B), has led some workers to conclude that subduction of atmospheric Ne is negligible (Holland and Ballentine, 2006; Péron et al., 2016; 2017).

In contrast, if Ne is subducted into the mantle in serpentinite related lithologies with $^{20}Ne/^{36}Ar$ ratios of similar to the values of 0.1-0.5 measured in antigorite-serpentinites and secondary peridotites (Fig 11); and 90-100% of the ^{36}Ar in the mantle has a subducted atmospheric origin (Holland and Ballentine, 2006); then we calculate that the primordial mantle must have had a $^{20}Ne/^{22}Ne$ ratio of at least 0.3-1.3 higher than the modern mantle (Fig 12). Furthermore, the maximum measured $^{20}Ne/^{22}Ne$ ratios of ~12.9 in Ocean Island Basalts from Iceland and the Galápagos (Mukhopadhyay, 2012; Péron et al., 2016; 2017), could be explained by mixing primordial mantle Ne derived from only the sun ($^{20}Ne/^{22}Ne = 13.4 \pm 0.2$; Heber et al., 2012) with subducted atmospheric Ne ($^{20}Ne/^{22}Ne = 9.8$) introduced in secondary peridotites (Fig 12). Similar proportions of subducted Xe are present in the mantle sources of OIB and MORB (Mukhopadhyay, 2012; Caracausi et al., 2016) and we suggest these reservoirs probably also contain similar proportions of up to ~10% subducted Ne. The lower

maximum measured $^{20}Ne/^{22}Ne$ of 12.5 in MORB compared to 12.9 in OIB probably reflects slightly different mixtures of primordial noble gases in these reservoirs. For example, the lower $^{20}Ne/^{22}Ne$ of the MORB source could indicate derivation of primordial Ne from both the Sun ($^{20}Ne/^{22}Ne$ >13.2) and Ne implanted in meteorites ($^{20}Ne/^{22}Ne$ = 12.5-12.7) (Fig 12). Nonetheless, our calculations suggest MORB Ne is unlikely to derive solely from meteorites and allowing for even minor subduction of atmospheric Ne (e.g. ~10% of the total Ne) favours the original presence of true Solar Ne in parts of the Earth's mantle. The incorporation of true Solar Ne in the mantle is significant because it requires an extensive magma ocean existed on the Early Earth before nebula gases had disipated (Mukhopadhyay, 2012; Tucker and Mukhopadhyay, 2014).

6. Conclusions

Noble gases and halogens in seafloor serpentinites and their metamorphosed equivalents in ophiolites record long histories of fluid alteration on the seafloor and during subduction. High concentrations of I and Br and high I/Cl and Br/Cl ratios provide evidence for fluid interaction with marine sediments, whereas elevated $^{40}Ar/^{36}Ar$ ratios of up to ~1000 in some ophiolites provide evidence for fluid interaction with terrigenous sediments on continental margins or in subduction zones. The strong enrichment of F/Cl and $^{20}Ne/^{36}Ar$ in chlorite harzburgites from both Cerro del Almirez and Cima di Gagnone provide evidence that slab fluids remobilise F and light noble gases during subduction and that these elements are retained in chlorite and fluid inclusions in secondary peridotites formed by antigorite breakdown.

Noble gases and halogens become progressively less abundant in serpentinites and their metamorphosed equivalents with increasing levels of dehydration. Bromine and I

appear to be preferentially lost relative to Cl during the initial stages of dehydration, but once fluid inclusion become the dominant hosts for these elements they are no longer fractionated. Noble gases are not strongly fractionated by diffusional mechanisms during metamorphism but they are redistributed between lithologies by advecting slab fluids. The relative abundances of volatiles delivered to the deep mantle is strongly dependent on a number of processes including original seafloor alteration, volatile compatibility in metamorphic minerals, chemical exchange between lithologies and the dehydration state of the slab when it is subducted beyond the arc. Subduction of seawater-derived volatiles into the deep mantle has previously been suggested to be sufficiently important that it dominates the mantle inventory of heavy noble gases and halogens and we suggest that it may also explain a change in the mantle's $^{20}Ne/^{22}Ne$ isotope signature from a primordial value of similar to the Sun (~13.4), to the current highest measured value of 12.9, demonstrating that subduction of volatiles exerts a major influence on interpretation of mantle noble gas systematics.

Acknowledgements

Dr M.A. Kendrick is supported by an ARC Future Fellowship (FT13 0100141). This work was made possible by the invaluable and expert technical support of Stanislav Szerepanski and Xiaodong Zhang in the noble gas laboratories at Melbourne University and the ANU respectively, and Pete Holden in the ANU SHRIMP laboratory. The authors acknowledge the facilities, and the scientific and technical assistance, of the Australian Microscopy & Microanalysis Research Facility at the Centre of Advanced Microscopy, the Australian National University. The manuscript was greatly improved by the constructive comments of three anonymous reviewers and the editorial suggestion of Mark Rehkämper.

References

Anselmi, B., Mellini, M., and Viti, C., 2000. Chlorine in the Elba, Monti Livornesi and Murlo serpentines: evidence for sea-water interaction. *European Journal of Mineralogy* **12**, 137-146.

Arnaud, N. O. and Kelley, S. P., 1995. Evidence for excess argon during high pressure metamorphism in the Dora Maira Massif (western Alps, Italy), using an ultra-violet laser ablation microprobe 40Ar-39Ar technique. *Contributions to Mineralogy and Petrology* **121**, 1-11.

Balcone-Boissard, H., Michel, A., and Villemant, B., 2009. Simultaneous Determination of Fluorine, Chlorine, Bromine and Iodine in Six Geochemical Reference Materials Using Pyrohydrolysis, Ion Chromatography and Inductively Coupled Plasma-Mass Spectrometry. *Geostandards and Geoanalytical Research* **33**, 477-485.

Ballentine, C. J., Marty, B., Lollar, B. S., and Cassidy, M., 2005. Neon isotopes constrain convection and volatile origin in the Earth's mantle. *Nature* **433**, 33-38.

Barnes, J. D., Manning, C. E., Scambelluri, M., and Selverstone, J., 2018. The behaviour of halogens during subduction zone processes. In: Harlov, D. E. and Aranovich, L. Y. Eds.), *The Role of Halogens in Terrestrial and Extraterrestrial Geochemical Processes*. Springer, Cham.

Bostock, M. G., Hyndman, R. D., Rondenay, S., and Peacock, S. M., 2002. An inverted continental Moho and serpentinization of the forearc mantle. *Nature* **417**, 536-538.

Brouwer, F. M., Burri, T., Engi, M., and Berger, A., 2005. Eclogite relics in the Central Alps: PT-evolution, Lu-Hf ages and implications for formation of tectonic melange zones. *Schweizerische Mineralogische Und Petrographische Mitteilungen* **85**, 147-174.

Cannaò, E., Agostini, S., Scambelluri, M., Tonarini, S., and Godard, M., 2015. B, Sr and Pb isotope geochemistry of high-pressure Alpine metaperidotites monitors fluid-mediated element recycling during serpentinite dehydration in subduction mélange (Cima di Gagnone, Swiss Central Alps). *Geochimica et Cosmochimica Acta* **163**, 80-100.

Cannaò, E., Scambelluri, M., Agostini, S., Tonarini, S., and Godard, M., 2016. Linking serpentinite geochemistry with tectonic evolution at the subduction plate-interface: The Voltri Massif case study (Ligurian Western Alps, Italy). *Geochimica et Cosmochimica Acta* **190**, 115-133.

Caracausi, A., Avice, G., Burnard, P. G., Füri, E., and Marty, B., 2016. Chondritic xenon in the Earth's mantle. *Nature* **533**, 82-85.

Chauvel, C., Hofmann, A. W., and Vidal, P., 1992. HIMU EM - The French-Polynesian Connection. *Earth and Planetary Science Letters* **110**, 99-119.

Chavrit, D., Burgess, R., Sumino, H., Teagle, D. A. H., Droop, G., Shimizu, A., and Ballentine, C. J., 2016. The contribution of hydrothermally altered ocean crust to the mantle halogen and noble gas cycles. *Geochimica et Cosmochimica Acta* **183**, 106-124.

Dalou, C. l., Koga, K., Shimizu, N., Boulon, J., and Devidal, J.-L., 2012. Experimental determination of F and Cl partitioning between lherzolite and basaltic melt. *Contributions to Mineralogy and Petrology* **163**, 591-609.

Debret, B., Koga, K. T., Nicollet, C., Andreani, M., and Schwartz, S., 2014. F, Cl and S input via serpentinite in subduction zones: implications for the nature of the fluid released at depth. *Terra Nova* **26**, 96-101.

Deschamps, F., Godard, M., Guillot, S., Chauvel, C., Andreani, M., Hattori, K., Wunder, B., and France, L., 2012. Behavior of fluid-mobile elements in serpentines from abyssal to subduction environments: Examples from Cuba and Dominican Republic. *Chemical Geology* **312,** 93-117.

Evans, B. W. and Trommsdorff, V., 1978. Petrogenesis of garnet lherzolite, Cima-di-Gagnone, Lepontine Alps. *Earth and Planetary Science Letters* **40**, 333-348.

Fehn, U., Snyder, G., and Egeberg, P. K., 2000. Dating of pore waters with I-129: Relevance for the origin of marine gas hydrates. *Science* **289**, 2332-2335.

Garrido, C. J., Sanchez-Vizcaino, V. L., Gomez-Pugnaire, M. T., Trommsdorff, V., Alard, O., Bodinier, J. L., and Godard, M., 2005. Enrichment of HFSE in chlorite-harzburgite produced by high-pressure dehydration of antigorite-serpentinite: Implications for subduction magmatism. *Geochem. Geophys. Geosyst.* **6**.

Gebauer D. (1996). A P-T-t path for an (ultra?-) high-pressure ultra mafic/mafic rock-association and its felsic country-rocks based on SHRIMP dating of magmatic and metamorphic zircon domains. Example: Alpe Arami (Central Swiss Alps). Earth Processes: Reading the Isotopic Code. American Geophysical Union, Geophysical Monographs 95, 309-328.

Gieskes, J. M., Simoneit, B. R. T., Goodfellow, W. D., Baker, P. A., and Mahn, C., 2002. Hydrothermal geochemistry of sediments and pore waters in Escanaba Trough—ODP Leg 169. *Applied Geochemistry* **17**, 1435-1456.

Green II, H. W., Chen, W.-P., and Brudzinski, M. R., 2010. Seismic evidence of negligible water carried below 400-km depth in subducting lithosphere. *Nature* **467**, 828-831.

Harvey, J., Garrido, C. J., Savov, I., Agostini, S., Padrón-Navarta, J. A., Marchesi, C., Sanchez-Vizcaino, V. L., and Gomez-Pugnaire, M. T., 2014. 11B-rich fluids in subduction zones: The role of antigorite dehydration in subducting slabs and boron isotope heterogeneity in the mantle. *Chemical Geology* **376**, 20-30.

Hattori, K. H. and Guillot, S., 2007. Geochemical character of serpentinites associated with high- to ultrahigh-pressure metamorphic rocks in the Alps, Cuba, and the Himalayas: Recycling of elements in subduction zones. *Geochem. Geophys. Geosyst.* **8**, 27.

Heber, V. S., Baur, H., Bochsler, P., McKeegan, K. D., Neugebauer, M., Reisenfeld, D. B., Wieler, R., and Wiens, R. C., 2012. Isotopic mass fractionatio of Solar Wind: Evidence from fast and slow Solar Wind collected by the Genesis Mission. *Astrophysical Journal* **759**.

Hermann, J., Fitz Gerald, J. D., Malaspina, N., Berry, A. J., and Scambelluri, M., 2007. OH-bearing planar defects in olivine produced by the breakdown of Ti-rich humite minerals from Dabie Shan (China). *Contributions to Mineralogy and Petrology* **153**, 417-428.

Hofmann, A. W., 2003. Sampling Mantle Heterogeneity through Oceanic Basalts: Isotopes and Trace Elements. In: Carlson, R. L. (Ed.), *Treatise of Geochemistry Volume 2: The Core and Mantle*. Elsevier Ltd.

Holland, G. and Ballentine, C. J., 2006. Seawater subduction controls the heavy noble gas composition of the mantle. *Nature* **441**, 186-191.

Holland, G., Cassidy, M., and Ballentine, C. J., 2009. Meteorite Kr in Earth's Mantle Suggests a Late Accretionary Source for the Atmosphere. *Science* **326**, 1522-1525.

Honda, M., Phillips, D., Harris, J. W., and Yatsevich, I., 2004. Unusual noble gas compositions in polycrystalline diamonds: preliminary results from the Jwaneng kimberlite, Botswana. *Chemical Geology* **203**, 347-358.

Hoskin, P. W. O., 1999. SIMS determination of mu g g(-1)-level fluorine in geological samples and its concentration in NIST SRM 610. *Geostandards Newsletter-the Journal of Geostandards and Geoanalysis* **23**, 69-76.

Jackson, C. R. M., Parman, S. W., Kelley, S. P., and Cooper, R. F., 2013. Noble gas transport into the mantle facilitated by high solubility in amphibole. *Nature Geosci* **6**, 562-565.

Jackson, C. R. M., Parman, S. W., Kelley, S. P., and Cooper, R. F., 2015. Light noble gas dissolution into ring structure-bearing materials and lattice influences on noble gas recycling. *Geochimica et Cosmochimica Acta* **159**, 1-15.

John, T., Scambelluri, M., Frische, M., Barnes, J. D., and Bach, W., 2011. Dehydration of subducting serpentinite: Implications for halogen mobility in subduction zones and the deep halogen cycle. *Earth and Planetary Science Letters* **308**, 65-76.

Kelley, S., 2002. Excess argon in K-Ar and Ar-Ar geochronology. *Chemical Geology* **188**, 1-22.

Kendrick, M. A., 2018. Halogens in seawater, marine sediments and the altered oceanic lithosphere. In: Harlov, D. E. and Aranovich, L. Y. Eds.), *The role of halogens in terrestrial and extraterrestrial processes* Springer. In Press.

Kendrick, M. A., 2012. High precision Cl, Br and I determination in mineral standards using the noble gas method. *Chemical Geology* **292-293**, 116-126.

Kendrick, M. A., Arculus, R. J., Burnard, P., and Honda, M., 2013a. Quantifying brine assimilation by submarine magmas: Examples from the Galápagos Spreading Centre and Lau Basin. *Geochimica et Cosmochimica Acta* **123**, 150-165.

Kendrick, M. A., Arculus, R. J., Danyushevsky, L., Kamenetsky, V. S., Woodhead, J., and Honda, M., 2014. Subduction-related halogens (Cl, Br and I) and H2O in magmatic glasses from Southwest Pacific Backarc Basins. *Earth and Planetary Science Letters* **400**, 165-176.

Kendrick, M. A. and Burnard, P., 2013. Noble gases and halogens in fluid inclusions: A journey through the Earth's crust. In: Burnard, P. (Ed.), *The Noble Gases as Geochemical Tracers*. Springer-Verlag, Berlin.

Kendrick, M. A., D'Andres, J., Holden, P., and Ireland, T., 2018. High Precision analyses of halogens (F, Cl, Br, I) in thirteen USGS, GSJ and NIST international rock powder and glass reference materials. *Geostandards and Geoanalytical Research*.

Kendrick, M. A., Hémond, C., Kamenetsky, V. S., Danyushevsky, L., Devey, C. W., Rodemann, T., Jackson, M. G., and Perfit, M. R., 2017. Seawater cycled throughout Earth's mantle in partially serpentinized lithosphere. *Nat. Geosci.* **10**, 222-228.

Kendrick, M. A., Honda, M., Pettke, T., Scambelluri, M., Phillips, D., and Giuliani, A., 2013b. Subduction zone fluxes of halogens and noble gases in seafloor and forearc serpentinites. *Earth and Planetary Science Letters* **365**, 86-96.

Kendrick, M. A., Honda, M., and Vanko, D. A., 2015. Halogens and noble gases in Mathematician Ridge meta-gabbros, NE Pacific: implications for oceanic hydrothermal root zones and global volatile cycles. *Contributions to Mineralogy and Petrology* **170**, 1-20.

Kendrick, M. A., Scambelluri, M., Honda, M., and Phillips, D., 2011. High abundances of noble gas and chlorine delivered to the mantle by serpentinite subduction. *Nat. Geosci.* **4**, 807-812.

Kobayashi, M., Sumino, H., Nagao, K., Ishimaru, S., Arai, S., Yoshikawa, M., Kawamoto, T., Kumagai, Y., Kobayashi, T., Burgess, R., and Ballentine, C. J., 2017. Slab-derived halogens and noble gases illuminate closed system processes controlling volatile element transport into the mantle wedge. *Earth and Planetary Science Letters* **457,** 106-116.

Kodolányi, J. and Pettke, T., 2011. Loss of trace elements from serpentinites during fluid-assisted transformation of chrysotile to antigorite - An example from Guatemala. *Chemical Geology* **284**, 351-362.

Kodolányi, J., Pettke, T., Spandler, C., Kamber, B. S., and Gméling, K., 2012. Geochemistry of Ocean Floor and Fore-arc Serpentinites: Constraints on the Ultramafic Input to Subduction Zones. *J. Petrol.* **53**, 235-270.

Kohlstedt, D. L., Keppler, H., and Rubie, D. C., 1996. Solubility of water in the alpha, beta and gamma phases of (Mg,Fe)(2)SiO4. *Contributions to Mineralogy and Petrology* **123**, 345-357.

Lafay, R., Fernandez-Martinez, A., Montes-Hernandez, G., Auzende, A. L., and Poulain, A., 2016. Dissolution-reprecipitation and self-assembly of serpentine nanoparticles preceding chrysotile formation: Insights into the structure of proto-serpentine. *Am. Miner.* **101**, 2666-2676.

López Sanchez-Vizcaino, V., Gomez-Pugnaire, M. T., Garrido, C. J., Padrón-Navarta, J. A., and Mellini, M., 2009. Breakdown mechanisms of titanclinohumite in antigorite serpentinite (Cerro del Almirez massif, S. Spain): A petrological and TEM study. *Lithos* **107**, 216-226.

López Sanchez-Vizcaino, V., Trommsdorff, V., Gomez-Pugnaire, M. T., Garrido, C. J., Muntener, O., and Connolly, J. A. D., 2005. Petrology of titanian clinohumite and olivine at the high-pressure breakdown of antigorite serpentinite to chlorite harzburgite (Almirez Massif, S. Spain). *Contributions to Mineralogy and Petrology* **149**, 627-646.

Marchesi, C., Garrido, C. J., Padrón-Navarta, J. A., Sanchez-Vizcaino, V. L., and Gomez-Pugnaire, M. T., 2013. Element mobility from seafloor serpentinization to high-pressure dehydration of antigorite in subducted serpentinite: Insights from the Cerro del Almirez ultramafic massif (southern Spain). *Lithos* **178**, 128-142.

Marks, M. A. W., Wenzel, T., Whitehouse, M. J., Loose, M., Zack, T., Barth, M., Worgard, L., Krasz, V., Eby, G. N., Stosnach, H., and Markl, G., 2012. The volatile inventory (F, Cl, Br, S, C) of magmatic apatite: An integrated analytical approach. *Chemical Geology* **291**, 241-255.

Matsuda, J. and Nagao, K., 1986. Noble-Gas Abundances in a Deep-Sea Sediment Core from Eastern Equatorial Pacific. *Geochem. J.* **20**, 71-80.

Michel, A. and Villemant, B., 2003. Determination of halogens (F, Cl, Br, I), sulfur and water in seventeen geological reference materials. Geostandards Newsletter-the Journal of *Geostandards and Geoanalysis* **27**, 163-171.

Moreira, M. and Charnoz, S., 2016. The origin of the neon isotopes in chondrites and on Earth. *Earth and Planetary Science Letters* **433**, 249-256.

Mukhopadhyay, S., 2012. Early differentiation and volatile accretion recorded in deep-mantle neon and xenon. *Nature* **486**, 101-104.

Muramatsu, Y., Doi, T., Tomaru, H., Fehn, U., Takeuchi, R., and Matsumoto, R., 2007. Halogen concentrations in pore waters and sediments of the Nankai Trough, Japan: Implications for the origin of gas hydrates. *Applied Geochemistry* **22**, 534-556.

Nadzri, A., Schauries, D., Mota-Santiago, P., Trautmann, C., Gleadow, A. J. W., Hawley, A., and Kluth, P., 2017. Composition and orientation dependent annealing of ion tracks in apatite - Implications for fission track thermochronology. *Chemical Geology* **451**, 9-16.

Nimis, P. and Trommsdorff, V., 2001. Revised thermobarometry of Alpe Arami and other garnet peridotites from the Central Alps. *J. Petrol.* **42**, 103-115.

Ozima, M. and Podosek, F. A., 2002. *Noble Gas Geochemistry*. Cambridge University Press.

Padrón-Navarta, J. A. and Hermann, J., 2017. A subsolidus Olivine Water Solubility Equation for the Earth's Upper Mantle. Journal of Geophysical Research **122**, 9862-9880.

Padrón-Navarta, J. A., Sanchez-Vizcaino, V. L., Garrido, C. J., and Gomez-Pugnaire, M. T., 2011. Metamorphic Record of High-pressure Dehydration of Antigorite Serpentinite to Chlorite Harzburgite in a Subduction Setting (Cerro del Almirez, Nevado-Filabride Complex, Southern Spain). *J. Petrol.* **52**, 2047-2078.

Padrón-Navarta, J. A., Sanchez-Vizcaino, V. L., Hermann, J., Connolly, J. A. D., Garrido, C. J., Gomez-Pugnaire, M. T., and Marchesi, C., 2013. Tschermak's substitution in antigorite and consequences for phase relations and water liberation in high-grade serpentinites. *Lithos* **178**, 186-196.

Padrón-Navarta, J. A., Tommasi, A., Garrido, C. J., and Mainprice, D., 2015. On topotaxy and compaction during antigorite and chlorite dehydration: an experimental and natural study. *Contributions to Mineralogy and Petrology* **169**.

Pagé, L., Hattori, K., de Hoog, J. C. M., and Okay, A. I., 2016. Halogen (F, Cl, Br, I) behaviour in subducting slabs: A study of lawsonite blueschists in western Turkey. *Earth and Planetary Science Letters* **442**, 133-142.

Pagé, L. and Hattori, K., 2017. Tracing halogen and B cycling in subduction zones based on obducted, subducted and forearc serpentinites of the Dominican Republic. *Scientific Reports* **7**.

Palme, H., O'Neill, H.S.C., 2003. Cosmochemical estimates of Mantle Composition. In: Holland, H., Turekian, K.K. (Eds.), Treatise on Geochemistry. Elsevier, New York, pp. 1-38.

Peters, D., Bretscher, A., John, T., Scambelluri, M., and Pettke, T., 2017. Fluid-mobile elements in serpentinites: Constraints on serpentinisation environments and element cycling in subduction zones. *Chemical Geology* **466**, 654-666.

Péron, S., Moreira, M., Colin, A., Arbaret, L., Putlitz, B., and Kurz, M. D., 2016. Neon isotopic composition of the mantle constrained by single vesicle analyses. *Earth and Planetary Science Letters* **449**, 145-154.

Péron, S., Moreira, M., Putlitz, B., and Kurz, M. D., 2017. Solar wind implantation supplied light volatiles during the first stage of Earth accretion. *Geochemical Perspectives Letters* **3**, 151-159.

Philippot, P., Agrinier, P., and Scambelluri, M., 1998. Chlorine cycling during subduction of altered oceanic crust. *Earth and Planetary Science Letters* **161**, 33-44.

Pitre, F. and Pinti, D. L., 2010. Noble gas enrichments in porewater of estuarine sediments and their effect on the estimation of net denitrification rates. *Geochimica et Cosmochimica Acta* **74**, 531-539.

Plumper, O., Royne, A., Magraso, A., and Jamtveit, B., 2012. The interface-scale mechanism of reaction-induced fracturing during serpentinization. *Geology* **40**, 1103-1106.

Podosek, F. A., Honda, M., and Ozima, M., 1980. Sedimentary Noble Gases. *Geochimica et Cosmochimica Acta* **44**, 1875-1884.

Puga, E., Nieto, J. M., de Federico, A. D., Bodinier, J. L., and Morten, L., 1999. Petrology and metamorphic evolution of ultramafic rocks and dolerite dykes of the Betic Ophiolitic Association (Mulhacen Complex, SE Spain): evidence of eo-Alpine subduction following an ocean-floor metasomatic process. *Lithos* **49**, 23-56.

Ranero, C. R., Phipps Morgan, J., McIntosh, K., and Reichert, C., 2003. Bending-related faulting and mantle serpentinization at the Middle America trench. *Nature* **425**, 367-373.

Raquin, A. and Moreira, M., 2009. Atmospheric Ar-38/Ar-36 in the mantle: Implications for the nature of the terrestrial parent bodies. *Earth and Planetary Science Letters* **287**, 551-558.

Risold, A. C., Trommsdorff, V., and Grobety, B., 2001. Genesis of ilmenite rods and palisades along humite-type defects in olivine from Alpe Arami. *Contributions to Mineralogy and Petrology* **140**, 619-628.

Roddick, J. C., 1983. High precision intercalibration of 40Ar-39Ar standards. *Geochimica et Cosmochimica Acta* **47**, 887-898.

Rude, P. D. and Aller, R. C., 1991. Fluorine mobility during early diagenesis of carbonate sediment: An indicator of mineral transformations. *Geochimica et Cosmochimica Acta* **55**, 2491-2509.

Sánchez-Vizcaíno, V. L., Rubatto, D., Gómez-Pugnaire, M. T., Trommsdorff, V., and Müntener, O., 2001. Middle Miocene high-pressure metamorphism and fast exhumation of the Nevado-Filábride Complex, SE Spain. *Terra Nova* **13**, 327-332.

Scaillet, S., 1996. Excess 40Ar transport scale and mechanism in high-pressure phengites: A case study from an eclogitized metabasite of the Dora-Maira nappe, western Alps. *Geochimica et Cosmochimica Acta* **60**, 1075-1090.

Scambelluri, M., Bottazzi, P., Trommsdorff, V., Vannucci, R., Hermann, J., Gòmez-Pugnaire, M. T., and Lòpez-Sànchez Vizcaino, V., 2001. Incompatible element-rich fluids released by antigorite breakdown in deeply subducted mantle. *Earth and Planetary Science Letters* **192**, 457-470.

Scambelluri, M., Fiebig, J., Malaspina, N., Müntener, O., and Pettke, T., 2004a. Serpentinite Subduction: Implications for Fluid Processes and Trace-Element Recycling. *International Geology Review* **46**, 595-613.

Scambelluri, M., Müntener, O., Hermann, J., Piccardo, G. B., and Trommsdorff, V., 1995. Subduction of water into the mantle - History of an Alpine Peridotite *Geology* **23**, 459-462.

Scambelluri, M., Müntener, O., Ottolini, L., Pettke, T. T., and Vannucci, R., 2004b. The fate of B, Cl and Li in the subducted oceanic mantle and in the antigorite breakdown fluids. *Earth and Planetary Science Letters* **222**, 217-234.

Scambelluri, M., Pettke, T., and Cannaò, E., 2015. Fluid-related inclusions in Alpine high-pressure peridotite reveal trace element recycling during subduction-zone dehydration of serpentinized mantle (Cima di Gagnone, Swiss Alps). *Earth and Planetary Science Letters* **429**, 45-59.

Scambelluri, M., Pettke, T., Rampone, E., Godard, M., and Reusser, E., 2014. Petrology and Trace Element Budgets of High-pressure Peridotites Indicate Subduction Dehydration of Serpentinized Mantle (Cima di Gagnone, Central Alps, Switzerland). *J. Petrol.* **55**, 459-498.

Scambelluri, M., Piccardo, G. B., Philippot, P., Robbiano, A., and Negretti, L., 1997. High salinity fluid inclusions formed from recycled seawater in deeply subducted alpine serpentinite. *Earth and Planetary Science Letters* **148**, 485-499.

Schmidt, M. W. and Poli, S., 1998. Experimentally based water budgets for dehydrating slabs and consequences for arc magma generation. *Earth and Planetary Science Letters* **163**, 361-379.

Seyfried, W. E. and Ding, K., 1995. The hydrothermal chemistry of fluoride in seawater. *Geochimica et Cosmochimica Acta* **59**, 1063-1071.

Sharp, Z. D. and Barnes, J. D., 2004. Water-soluble chlorides in massive seafloor serpentinites: a source of chloride in subduction zones. *Earth and Planetary Science Letters* **226**, 243-254.

Sherlock, S. and Kelley, S., 2002. Excess argon evolution in HP-LT rocks: a UVLAMP study of phengite and K-free minerals, NW Turkey. *Chemical Geology* **182**, 619-636.

Smye, A. J., Jackson, C. R. M., Konrad-Schmolke, M., Hesse, M. A., Parman, S. W., Shuster, D. L., and Ballentine, C. J., 2017. Noble gases recycled into the mantle through cold subduction zones. *Earth and Planetary Science Letters* **471**, 65-73.

Sumino, H., Burgess, R., Mizukami, T., Wallis, S. R., Holland, G., and Ballentine, C. J., 2010. Seawater-derived noble gases and halogens preserved in exhumed mantle wedge peridotite. *Earth and Planetary Science Letters* **294**, 163-172.

Sun, W. D., Binns, R. A., Fan, A. C., Kamenetsky, V. S., Wysoczanski, R., Wei, G. J., Hu, Y. H., and Arculus, R. J., 2007. Chlorine in submarine volcanic glasses from the eastern Manus basin. *Geochimica Et Cosmochimica Acta* **71**, 1542-1552.

Tomaru, H., Fehn, U., Lu, Z. L., and Matsumoto, R., 2007. Halogen systematics in the Mallik 5L-38 gas hydrate production research well, Northwest Territories, Canada: Implications for the origin of gas hydrates under terrestrial permafrost conditions. *Applied Geochemistry* **22**, 656-675.

Trieloff, M., Kunz, J., Clague, D. A., Harrison, D., and Allegre, C. J., 2000. The nature of pristine noble gases in mantle plumes. *Science* **288**, 1036-1038.

Trommsdorff, V., Sanchez-Vizcaino, V. L., Gomez-Pugnaire, M. T., and Muntener, O., 1998. High pressure breakdown of antigorite to spinifex-textured olivine and orthopyroxene, SE Spain. *Contributions to Mineralogy and Petrology* **132**, 139-148.

Tucker, J. M. and Mukhopadhyay, S., 2014. Evidence for multiple magma ocean outgassing and atmospheric loss episodes from mantle noble gases. *Earth and Planetary Science Letters* **393,** 254-265.

Vignaroli, G., Rossetti, F., Rubatto, D., Theye, T., Lisker, F., and Phillips, D., 2010. Pressure-temperature-deformation-time (P-T-d-t) exhumation history of the Voltri Massif HP complex, Ligurian Alps, Italy. *Tectonics* **29**, n/a-n/a.

Workman, R.K., Hart, S.R., 2005. Major and trace element composition of the depleted MORB mantle (DMM). *Earth and Planetary Science Letters*, **231**(1-2): 53-72.

Yokochi, R. and Marty, B., 2004. A determination of the neon isotopic composition of the deep mantle. *Earth and Planetary Science Letters* **225**, 77-88.

Table 1. Summary of halogens in serpentinites and their metamorphosed equivalents

	K ppm	Cl ppm	Br ppb	I ppb	F ppm	Br/Cl $\times10^{-3}$	I/Cl $\times10^{-6}$
	Noble gas method on mineral separates					SIMS	
Oceanic serpentinites							
Seafloor (n = 9)[1]	4-74	460-1700	1300-6800	17-580	<20	2.7-5.6	28-1300
Fore-arc (n = 8)[1]	13-270	420-2300	2700-24,000	2100-45,000	nd	5.3-10.4	1900-43,000
Erro Tobbio (n = 3)[1]	<37	330-740	1300-3400	490-1300	<20	3.8-4.6	870-1900
Antigorite serpentinites							
Erro Tobbio (n = 5)[2]	8-63	75-570	260-2100	41-180	<20	2.4-4.1	170-790
Cerro del Almirez							
Alm94	12	220	170	20	~20	0.75	90
Alm119	7	250	300	24	<20	1.2	97
Alm125	23	160	220	13	<20	1.4	78
Chlorite harzburgites							
Cerro del Almirez							
Spinifex rocks (n = 2)[2]	7-130	95-380	110-810	4-72	36-170	1.0-2.1	46-190
Chl-rich veins (n = 2)[2]	9-29	67-360	66-310	5-25	180-270	0.7-1.0	52-79
Al08-16 ol/en –a	27	170	220	27	16 ± 11	1.3	160
Al08-16 ol/en –b	24	200	220	29		1.1	150
Al08-16 chl –a	28	150	140	43	240 ± 30	0.90	290
Al08-16 chl –b	25	150	130	42		0.87	290
Al08-16 chl –c	34	150	140	47		0.93	310
Al08-16 WR	26*	180*	210*	31*	49	1.2*	170*
Al10-06 ol/en –a	16	240	360	26		1.6	110
Al10-06 ol/en –b	15	220	340	22		1.6	100
Al10-06 chl –a	12	140	200	44		1.5	330
Al10-06 chl –b	9	140	170	41		1.2	300
Al10-06 WR	15*	210*	330*	27*	78	1.6*	130*
Cima di Gagnone							
Mg31 09-03	6	36	320	7	39	8.6	210
Garnet peridotite, Cima di Gagnone							
Mg160 - grt	9	78	360	14	5 ± 1	4.6	170
Mg160 - ol-en	nd	20	100	8	13 ± 2	5.2	380
Mg160 - cpx	230	290	980	33	10 ± 5	3.3	110
Mg160 – WR		~60*	~260*	~12*	~11*	~4.1*	~190*
Mg160 - Peak		~40*	~180*	~9*	~11*	~4.8*	~260*
Reference values							
Seawater	0.038	19,300	66,000	58	1.3	3.5	3.5
Mantle[3]	40-80	5 ± 2	13 ± 6	0.3 ± 0.1	12 ± 2	2.8 ± 0.8	60 ± 30
Primitive mantle[3]	260 ± 80	26 ± 8	76 ± 25	7 ± 4	17 ± 6	2.9 ± 0.6	270 ±120

Analyses are 'total fusion' values based on the total gas released in all heating steps, the data are reported fully in the Electronic Supplement.

[1]*Data ranges summarised from Kendrick et al. (2013).*

[2]*Data ranges summarised from Kendrick et al. (2011).*

[3]*Reference values from (Kendrick et al., 2017; Palme and O'Neill, 2003; Workman and Hart, 2005).*

**estimated: Chlorite harzburgites are assumed to have 15(chl):85(ol-en). Mg160 – WR is estimated based on the model mineralogy (65(Ol+en):25 (grt): 10 (cpx + hbl)), whereas the cpx mineral separate is not included in Mg160 – Peak (65(Ol+en):25 (grt))*

Table 2. Noble gases in irradiated serpentinites and their metamorphosed equivalents

	^{36}Ar mol/g $\times10^{-15}$	^{84}Kr/^{36}Ar	^{130}Xe/^{36}Ar	^{40}Ar/^{36}Ar
Oceanic serpentinites				
Seafloor (n = 9)[1]	80-5,400	0.026-0.056	0.00030-0.00124	303-380
Fore-arc (n = 8)[1]	210-4,000	0.029-0.044	0.00046-0.00106	307-342
Erro Tobbio (n = 3)[1]	550-1400	0.025-0.030	0.00023-0.00033	320-322
Antigorite serpentinites				
Erro Tobbio (n = 5)[2]	210-740	0.03-0.05	0.0004-0.0011	311-390
Cerro del Almirez				
Alm94	750	0.035 ± 0.003	0.00056 ± 0.00005	321 ± 4
Alm119	330	0.034 ± 0.003	0.00048 ± 0.00005	375 ± 10
Alm125	430	0.026 ± 0.002	0.00025 ± 0.00003	390 ± 23
Chlorite harzburgites				
Cerro del Almirez				
Spinifex rocks (n = 2)[2]	52-260	0.07-0.10	0.0014-0.0041	360-510
Chl.-rich veins (n =2)[2]	21-220	0.05-0.08	0.0009-0.0018	375-700
Al08-16 ol/en –a	70	0.054 ± 0.010	0.00187 ± 0.00038	379 ± 59
Al08-16 ol/en –b	9.4	0.045 ± 0.036	0.00209 ± 0.00205	690 ± 530
Al08-16 chl –a	470	0.028 ± 0.003	0.00064 ± 0.00009	311 ± 23
Al08-16 chl –b	640	0.028 ± 0.003	0.00053 ± 0.00003	297 ± 7
Al08-16 chl –c	320	0.028 ± 0.004	0.00079 ± 0.00015	299 ± 33
Al10-06 ol/en –a	66	0.039 ± 0.011	0.00103 ± 0.00033	380 ± 100
Al10-06 ol/en –b	54	0.045 ± 0.015	0.00108 ± 0.00039	410 ± 130
Al10-06 chl –a	220	0.036 ± 0.005	0.00126 ± 0.00018	294 ± 26
Al10-06 chl –b	210	0.037 ± 0.005	0.00124 ± 0.00015	305 ± 21
Cima di Gagnone				
Mg31 09-03	290	0.033 ± 0.003	0.00052 ± 0.00007	382 ± 17[†]
Garnet peridotite, Cima di Gagnone				
Mg160 - grt	46	0.044 ± 0.005	0.00096 ± 0.00033	1080 ± 270
Mg160 - ol-en	24	0.046 ± 0.026	0.00200 ± 0.00117	720 ± 400
Mg160 - cpx	110	0.045 ± 0.006	0.00074 ± 0.00014	1160 ± 90
Mg160 – WR	~40*	~0.045*	~0.001*	~1000*
Mg160 - Peak	~30*	~0.045*	~0.001*	~900*

Analyses exclude low temperature heating steps (e.g. 300 or 400 °C). Uncertainties are 2σ. Data are reported fully in the Electronic Supplement. [1]Data ranges summarised from Kendrick et al. (2013). [2]Data ranges summarised from Kendrick et al. (2011). [†]This *value is lower than the value of 646 ± 2 in the non-irradiated aliquot (Table 3) and is attributed to persistent atmospheric contamination, see text.*

Table 3. Noble gases in non-irradiated serpentinites and their metamorphosed equivalents

	^{36}Ar mol/g $\times 10^{-15}$	^{4}He/^{36}Ar	^{20}Ne/^{36}Ar	^{84}Kr/^{36}Ar	^{130}Xe/^{36}Ar	^{40}Ar/^{36}Ar
Oceanic serpentinites						
Seafloor (n = 4)[1]	110-630	2.1-109	0.02-0.10	nd	nd	296-317
Fore-arc (n = 2)[1]	500-630	0.2-0.9	0.13-0.19	nd	nd	~296
Antigorite serpentinites						
Erro Tobbio (n = 3)[2]	90-590	~8	0.06-0.10	0.029-0.044	0.00056-0.0015	308-332
Cerro del Almirez						
Alm94	65	2760 ± 220	0.11 ± 0.10	0.019 ± 0.002	0.00087 ± 0.00008	372 ± 10
Alm125	130	1800 ± 140	0.22 ± 0.04	0.024 ± 0.002	0.00036 ± 0.00004	509 ± 6
Chlorite harzburgites						
Cerro del Almirez						
Spinifex rocks (n = 2)[2]	18-110	1620	0.075-0.53	0.028-0.063	0.00032-0.0033	370-633
Veins (n = 2)[2]	43-120	nd	0.18-0.32	0.039-0.055	0.00060-0.0013	373-536
Al08-16 ol/en	66	6100 ± 2600	0.17 ± 0.04	0.079 ± 0.009	0.00640 ± 0.00150	488 ± 4
Al08-16 chl	230	800 ± 320	0.25 ± 0.06	0.020 ± 0.004	0.00144 ± 0.00030	308 ± 36
Al10-06 WR	130	2370 ± 380	0.11 ± 0.02	0.036 ± 0.003	0.00559 ± 0.00053	340 ± 2
Cima di Gagnone						
Mg31 09-03	180	1600 ± 690	0.27 ± 0.04	0.027 ± 0.003	0.00073 ± 0.00010	646 ± 2
Garnet peridotite, Cima di Gagnone						
Mg160-WR	56	1160 ± 90	0.21 ± 0.04	nd	0.00077 ± 0.00012	935 ± 10
Reference values						
Atmosphere	-	0.17	0.52	0.021	0.00011	296
Seawater 25 °C	34,000	0.05	0.17	0.036	0.00035	296
Mantle	~2	3000-7000	~1.4	~0.06	~0.001	~10,000-30,000

Analyses are based on total fusion in a single heating step at 1500, 1600 or 1800 °C. Uncertainties are 2σ. Data are reported fully in the Electronic Supplement.

[1]*Data ranges summarised from Kendrick et al. (2013).*

[2]*Data ranges summarised from Kendrick et al. (2011).*

[3]*Reference values from Ozima and Podosek (2002).*

Fig 1 (Kendrick et al., 2018)

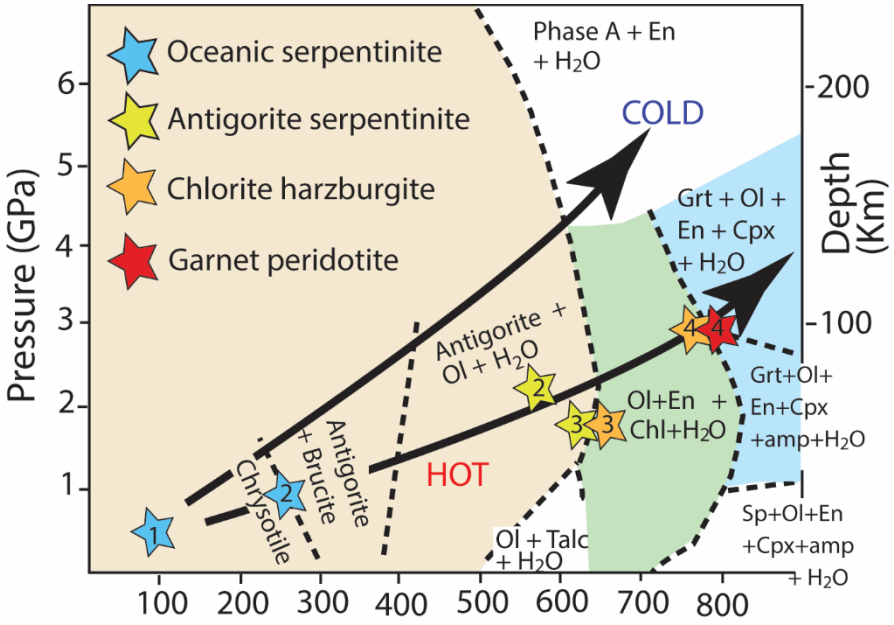

Fig 1. Schematic phase diagram showing the relationships between mineral phases in oceanic serpentinites formed on the seafloor and their metamorphosed equivalents. The diagram is modified from Scambelluri et al. (2004) and (2014). Hot and cold subduction geotherms are shown for reference (Peacock, 1990). Note that the exact positions of the phase boundaries and mineral assemblages vary with composition (see pseudosections in Scambelluri et al. (2014)). Investigated locations include: (1) Monte Nero and IODP seafloor serpentinites; (2) Erro Tobbio; (3) Cerro del Almirez; (4) Cima di Gagnone.

Fig 2 (Kendrick et al., 2018)

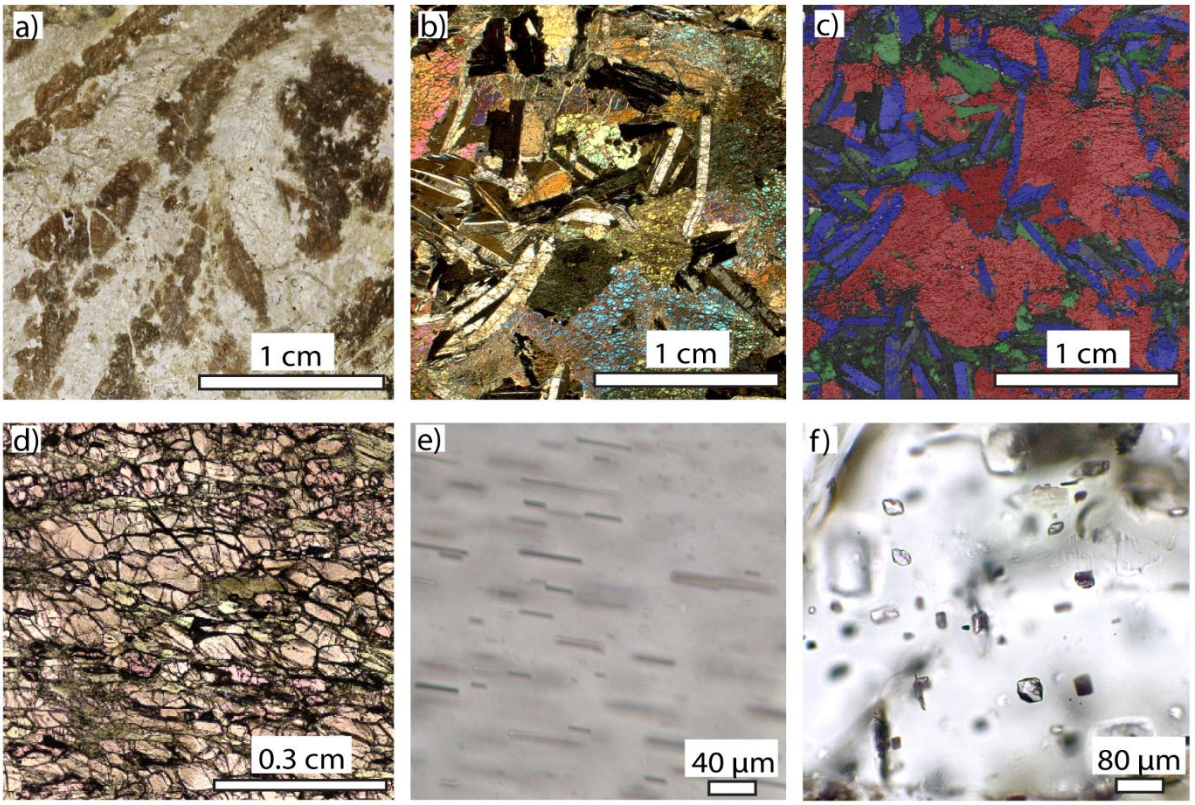

Fig 2. Photomicrographs of representative peridotite samples. a) a spinifex textured chlorite harzburgite (Alm8) with skeletal brown olivine in an enstatite dominated matrix. b and c) A granofels chlorite harzburgite (Al10-06) with abundant chlorite clots and false colour (blue = enstatite, red = olivine, green = chlorite). d) Garnet peridotite Mg160. e) Ilmenite needles in olivine of sample Mg160. f) a representative example of desiccated fluid inclusion remnants in a sample from Mg160. Images a, d, e, f are plain polars, image b is crossed polars.

Fig 3 (Kendrick et al., 2018)

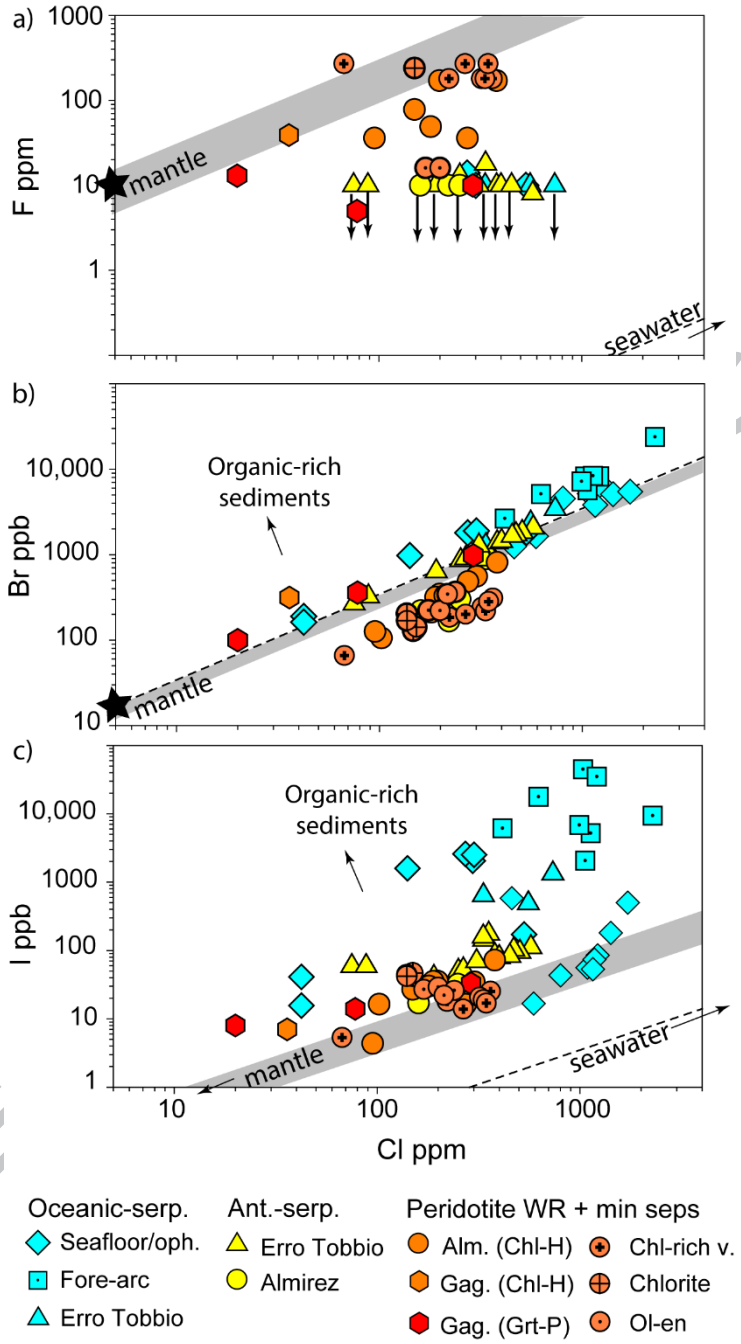

Fig 3. Halogen concentrations in serpentinites, secondary peridotites and mineral separates. The average concentrations of F, Cl and Br in the depleted mantle is shown by the black stars. The F/Cl, Br/Cl and I/Cl ratios of the mantle (grey fields) and seawater (dashed lines) are also shown (Drever, 1997; Kendrick et al., 2017). Abbreviations: serp. = serpentinite; oph. = ophiolite; Ant.-serp. = antigorite serpentinite, Peridotite WR + min seps = peridotite whole rock and mineral separates; Alm. (Chl-H) = chlorite harzburgite, Cerro del Almirez; Gag. (Chl-H) = Chlorite harzburgite, Cima di Gagnone; Gag. (Gnt-P) = garnet peridotite, Cima di Gagnone; Chl-rich v. = chlorite rich vein; ol-ens = olivine-enstatite.

Fig 4 (Kendrick et al., 2018)

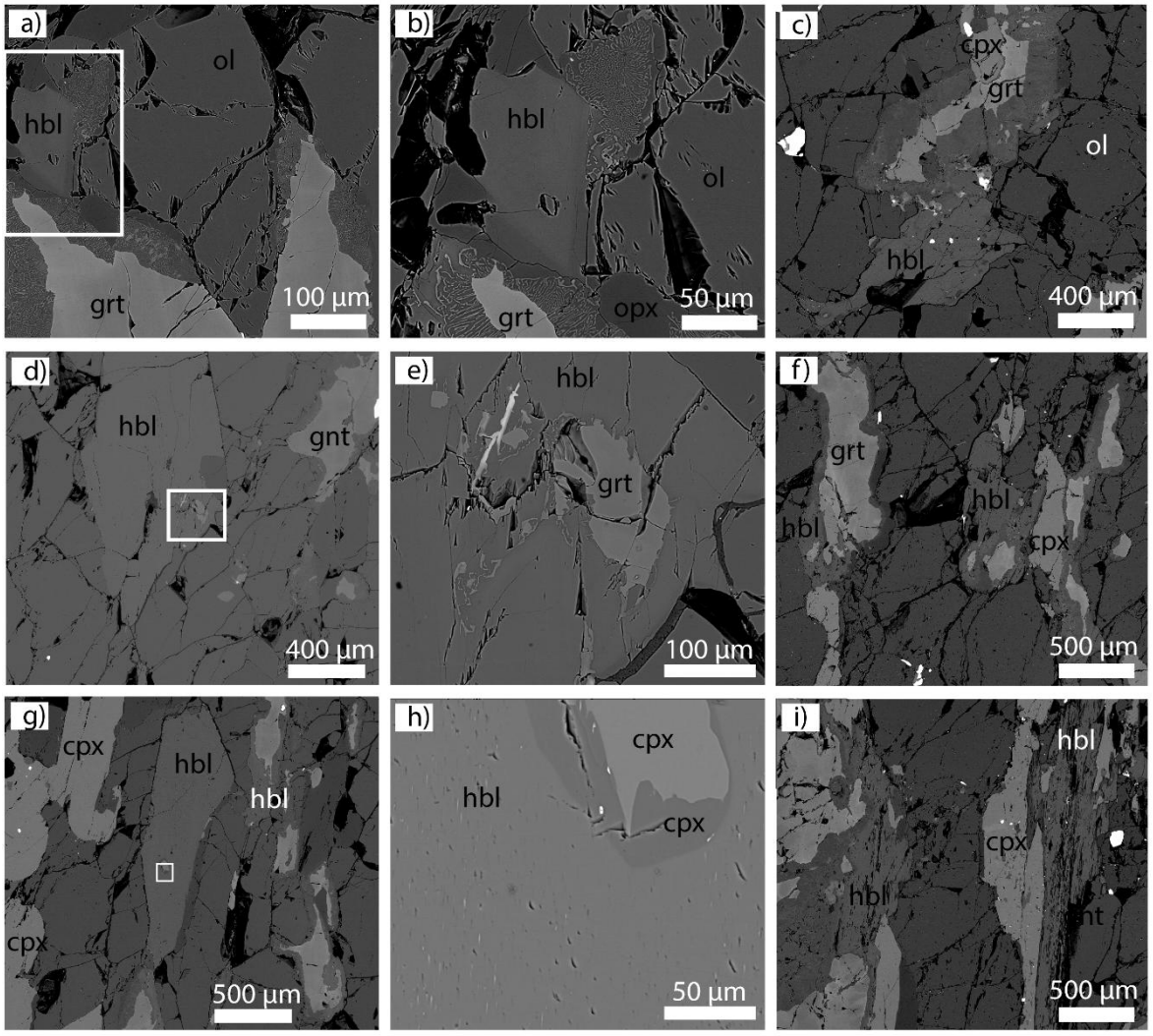

Fig 4. Backscattered electron images of secondary hornblendes in sample Mg160. a) hornblende (hbl-3) closely associated with kelyphite rims on garnet. B) an enlargement of the box in 'a' showing complete replacement of garnet in the upper right portion. c) hornblende (hbl-18) next to a kelyphite rim with a small garnet core. d) a mm-sized hornblende (hbl-14) with garnet inclusion. e) an enlargement of the box in d showing the replacement of the garnet inclusion. f) hornblende (hbl-19) associated with garnet and clinopyroxene. g) a mm-sized hornblende (hbl-15) with a clinopyroxene inclusion. h) an enlargement of the box in part f showing the clinopyroxene inclusion has been eroded by replacement and has a dark reaction rim. Brightly coloured lamellae in the hornblende provide further evidence for its replacive origin. i) elongated hornblende (hbl-20) adjacent to clinopyroxene. Hornblende compositions are given in the electronic supplement.

Fig 5 (Kendrick et al., 2018)

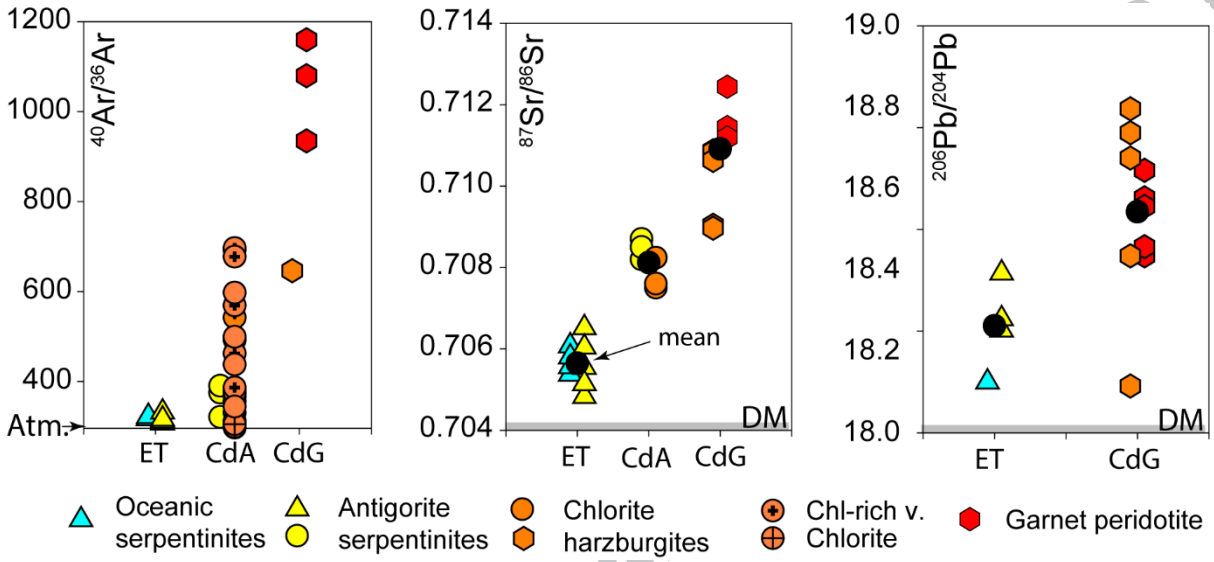

Fig 5. The $^{40}Ar/^{36}Ar$ of serpentinites and related rocks from Erro Tobbio (ET), Cerro del Almirez (CdA) and Cima di Gagnone (CdG) together with previously published $^{87}Sr/^{86}Sr$ and $^{206}Pb/^{204}Pb$ data (Harvey et al., 2014; Cannaò et al., 2015). The black circles indicate the mean $^{87}Sr/^{86}Sr$ and $^{206}Pb/^{204}Pb$ ratios for each locality. Note that all ophiolite samples are enriched in radiogenic ^{40}Ar relative to seawater and ^{87}Sr and ^{206}Pb compared to the depleted mantle (DM). Abbreviations: Atm. = atmosphere/seawater; Chl.-rich v. = chlorite rich vein.

Fig 6 (Kendrick et al., 2018)

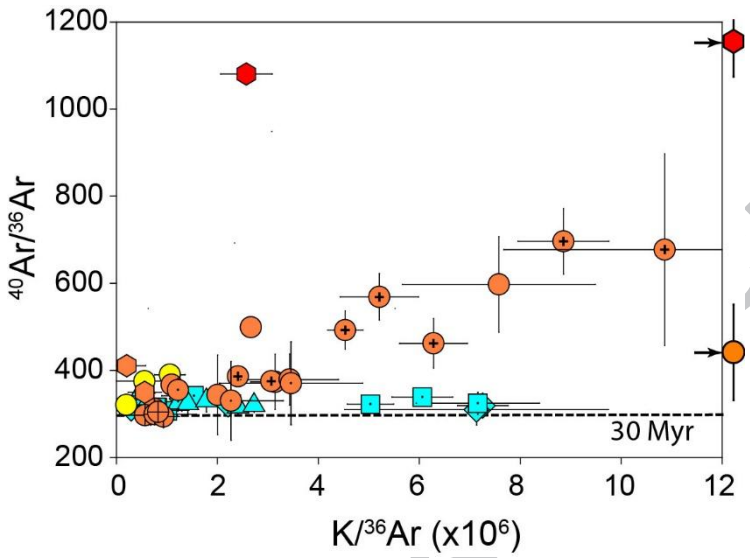

Fig 6. $K/^{36}Ar$ versus $^{40}Ar/^{36}Ar$ for samples with measurable K. The slope of a 30 Myr isochron shown as a dotted line falls in the Alpine orogeny, peak metamorphism is indicated to have been ~15 Ma at Cerro del Almirez (Sánchez-Vizcaíno et al., 2001), ~30 Ma at Erro Tobbio (Vignaroli et al., 2010) and ~35-45 Ma at Cima di Gagnone (Gebauer, 1996; Brouwer et al., 2005). This shows the samples contain negligible ^{40}Ar produced by in situ radioactive decay of ^{40}K and the measured $^{40}Ar/^{36}Ar$ ratios are representative of the initial values trapped in the samples during alteration. Data symbols are the same as in Fig 3, uncertainties are 2σ.

Fig 7 (Kendrick et al., 2018)

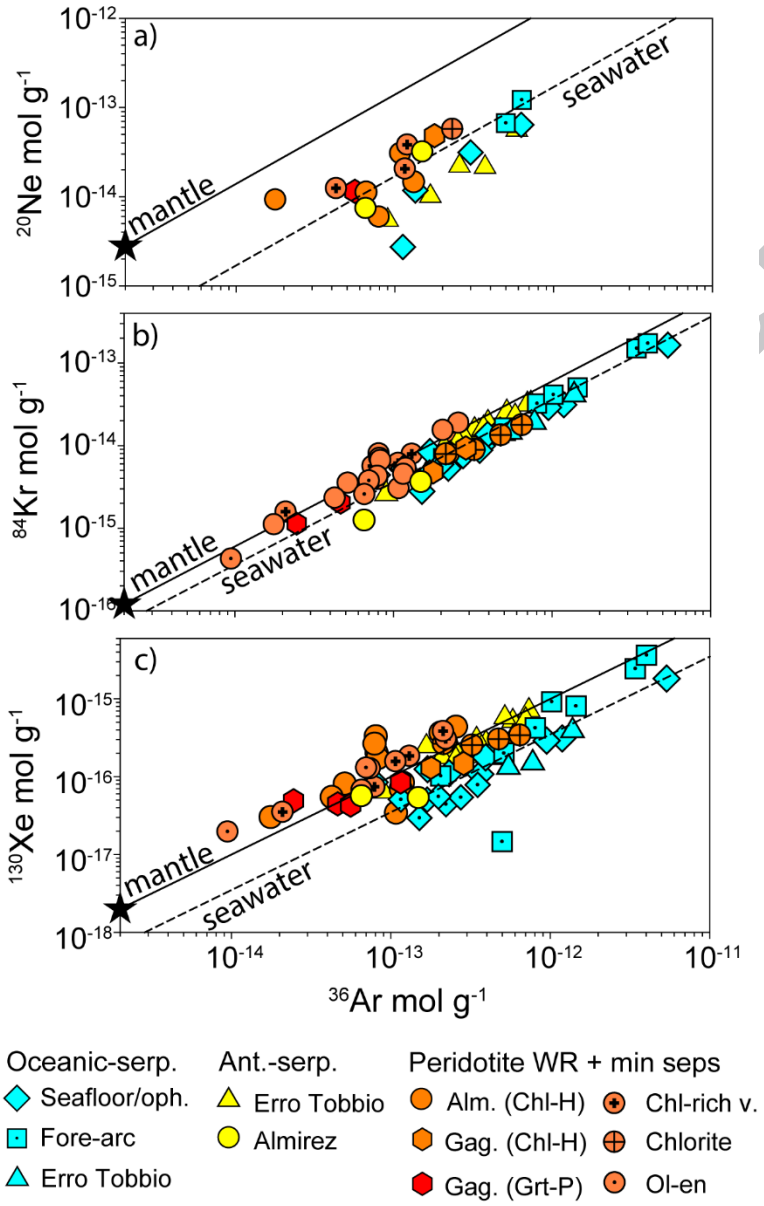

Fig 7. Noble gas concentrations in serpentinites, secondary peridotites and mineral separates. Note that the mantle concentrations of ^{36}Ar, ^{20}Ne, ^{84}Kr and ^{130}Xe estimated by Holland and Ballentine (2006) and slopes representing the $^{20}Ne/^{36}Ar$, $^{84}Kr/^{36}Ar$ and $^{130}Xe/^{36}Ar$ ratios of the mantle and seawater are shown for reference. Abbreviations are defined in Fig 3.

Fig 8 (Kendrick et al., 2018)

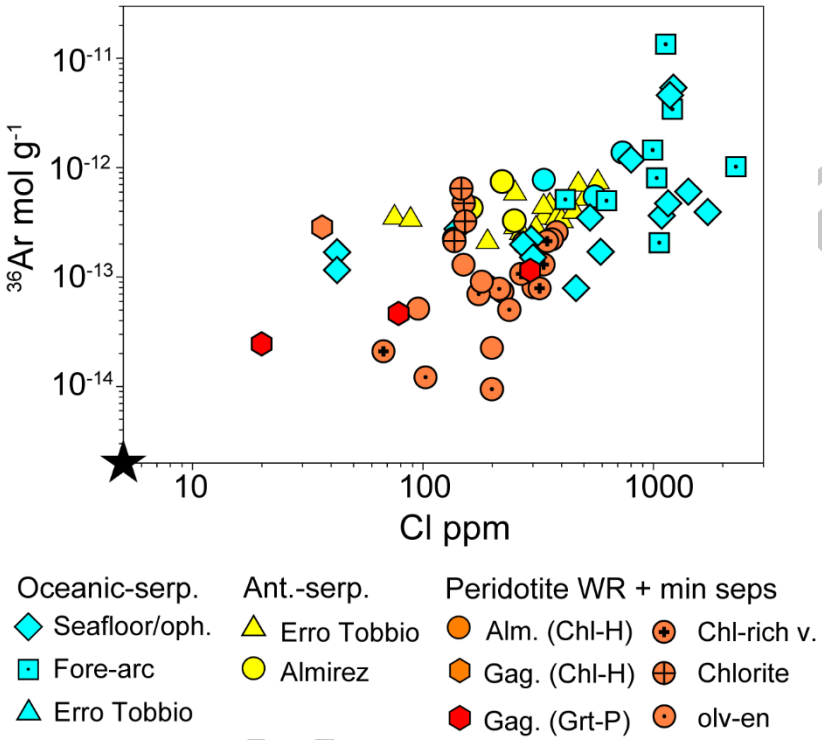

Fig 8. The concentration of Cl versus ^{36}Ar in serpentinites, secondary peridotites and mineral separates. Depleted mantle Cl and ^{36}Ar concentrations are from Holland and Ballentine (2006) and Kendrick et al. (2017). Abbreviations are defined in Fig 3.

Fig 9 (Kendrick et al., 2018)

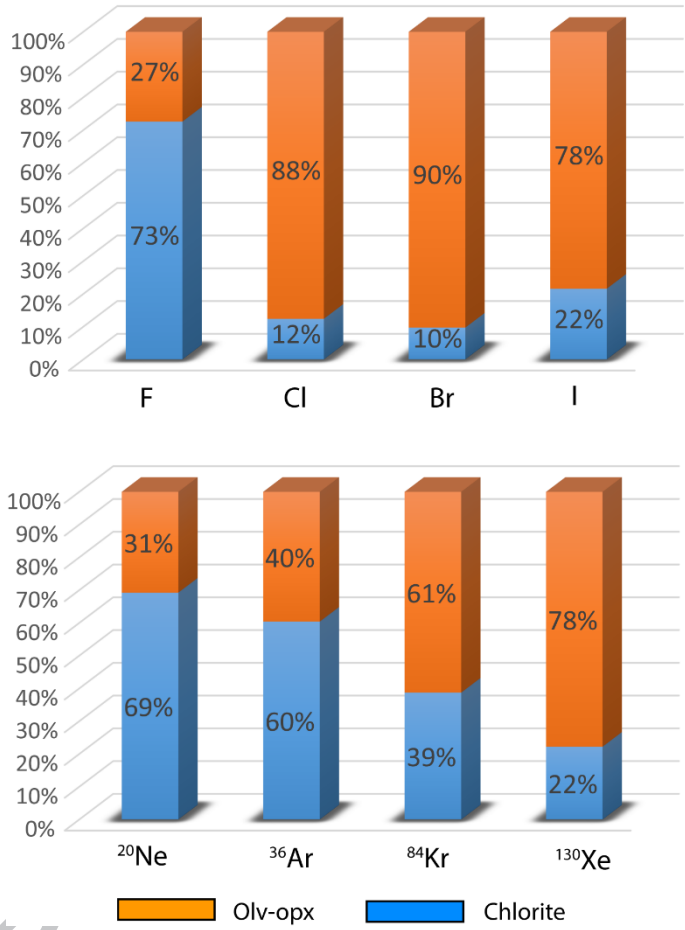

Fig 9. Stacked bar chart showing the distribution of halogens and atmospheric noble gases in the chlorite harzburgite sample Al08-16. Chlorite with a modal abundance of 15% does not host visible fluid inclusions, whereas olivine and enstatite host desiccated fluid inclusions (Fig 2f). Note that noble gas concentrations are based on the averages in irradiated and non-irradiated samples (average ^{20}Ne = average $^{36}Ar \times {}^{20}Ne/{}^{36}Ar_{non\text{-}irradiated}$).

Fig 10 (Kendrick et al., 2018)

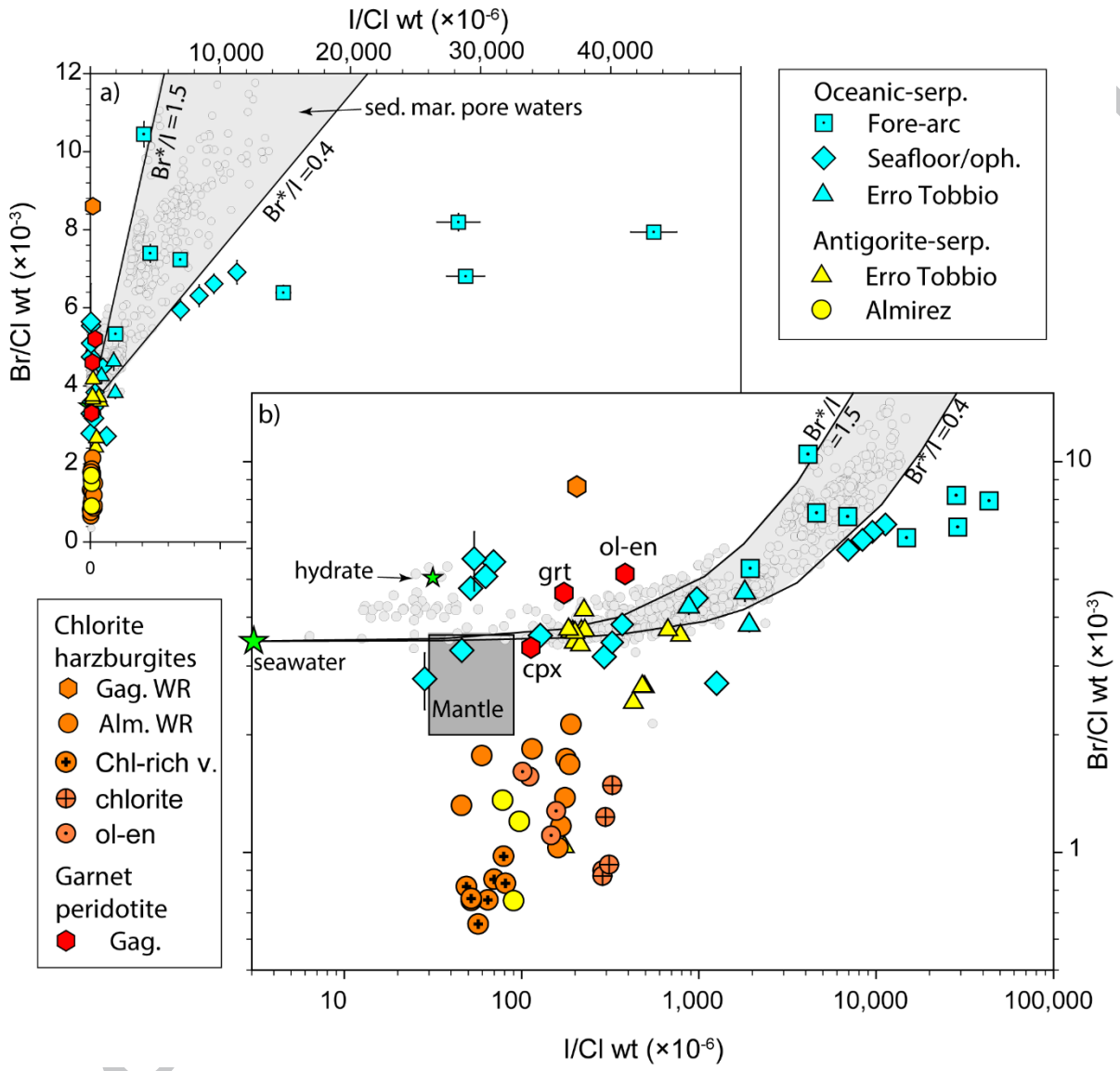

Fig 10. The Br/Cl and I/Cl ratios of serpentinites, secondary peridotites and mineral separates shown in both linear space (a) and log-log (b) space. Abbreviations: serp. = serpentinite; oph. = ophiolite; Gag. WR = Cima di Gagnone whole rock; Alm. WR = Cerro del Almirez whole rock; Chl.-rich v. = chlorite rich vein; ol-ens = olivine-enstatite; gnt = garnet; cpx = clinopyroxene; Gag = Cima di Gagnone. The compositional ranges of seawater, sedimentary pore waters (e.g. Fehn et al., 2000; Muramatsu et al., 2007; Tomaru et al., 2007, see Kendrick, 2018 for review) and the mantle (Kendrick et al., 2013a; 2017) are shown for reference.

Fig 11 (Kendrick et al., 2018)

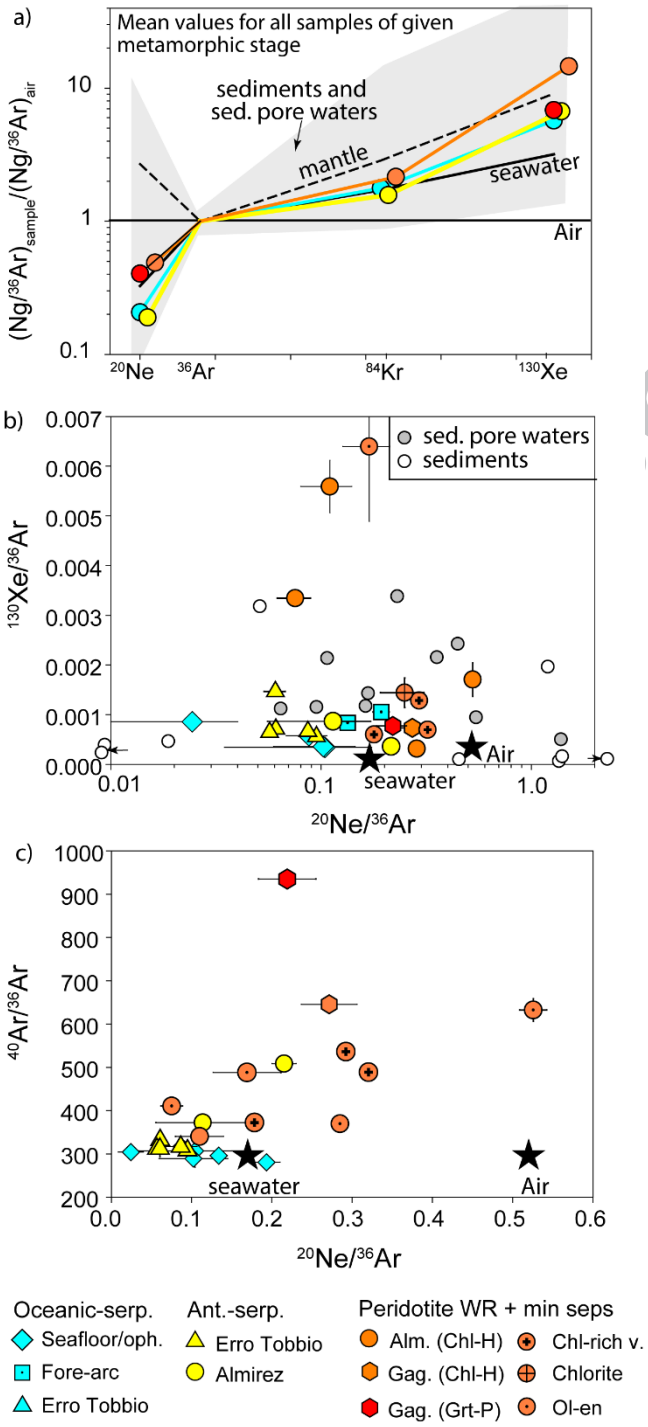

Fig 11. Noble gas abundance ratios for serpentinites, secondary peridotites and mineral separates. a) Average noble gas fractionation values [(Ng/^{36}Ar) normalised to air] for i) oceanic serpentinites (blue), ii) antigorite serpentinites (yellow), iii) chlorite harzburgites (orange), iv) garnet peridotite (red). b) ^{20}Ne/^{36}Ar versus ^{130}Xe/^{36}Ar, including the composition of sedimentary pore waters (Pitre and Pinti, 2010) and sediments (Podosek et al., 1980; Matsuda and Nagoa, 1986). c) ^{20}Ne/^{36}Ar versus ^{40}Ar/^{36}Ar, showing high ^{20}Ne/^{36}Ar ratios are not a result of atmospheric contamination. Seawater, the mantle and air from Ozima and Podosek (2002) and Holland and Ballentine (2002). Abbreviations as defined in Fig 3 except sed. pore waters = sedimentary pore waters.

Fig 12 (Kendrick et al., 2018)

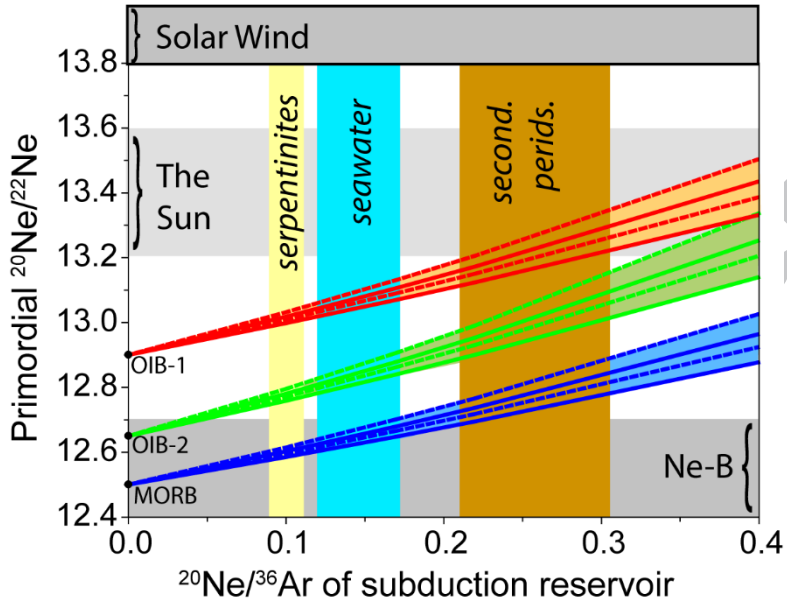

Fig 12. Plot showing how the mantle's $^{20}Ne/^{22}Ne$ ratio (y axis) could have been modified by subduction of reservoirs with different $^{20}Ne/^{36}Ar$ (x axis). The modern mantle has a maximum measured $^{20}Ne/^{22}Ne$ of 12.9 (OIB-1) that is lower than the Sun's value of >13.2 (Mukhopadhyay, 2012; Heber et al., 2012; Péron et al., 2016). The primordial $^{20}Ne/^{22}Ne$ could only be preserved in the mantle if average subduction reservoirs have $^{20}Ne/^{36}Ar$ close to 0. Higher average $^{20}Ne/^{36}Ar$ ratios of subduction reservoirs imply a higher primordial $^{20}Ne/^{22}Ne$ ratio (projected lines). The red lines projected from the maximum measured $^{20}Ne/^{22}Ne$ of the modern mantle intersect the area of overlap between 'The Sun' and 'secondary peridotite' showing that $^{20}Ne/^{22}Ne$ of 12.9 could be generated by mixing Solar neon and subducted atmospheric neon introduced into the mantle in secondary peridotite. The different lines generated for each mantle composition (OIB-1, OIB-2, MORB) are based on different estimates of mantle $^{20}Ne/^{36}Ar$ (Popping rock or Bravo dome; Holland and Ballentine, 2006) and assuming either 90 or 100% of ^{36}Ar has a subducted origin in the Earth's mantle.